UCRL-JRNL-218795

LAWRENCE LIVERMORE NATIONAL LABORATORY

Titan Imagery with Keck AO during and after Probe Entry

I. de Pater, M. Adamkovics, A. H. Bouchez, M. E. Brown, S. G. Gibbard, F. Marchis, H. G. Roe, E. L. Schaller, E. Young

February 9, 2006

Geophysical Research Planets

Titan Imagery with Keck AO during and after Probe Entry

Imke de Pater[1], Máté Ádámkovics[1], Antonin H. Bouchez[2]

Michael E. Brown[3], Seran G. Gibbard[4], Franck Marchis[1],

Henry G. Roe[3], Emily L. Schaller[3], and Eliot Young[5]

1. Department of Astronomy, 601 Campbell Hall

University of California, Berkeley CA 94720

2. Caltech Optical Observatories

California Institute of Technology, Pasadena, CA 91125

3. Division of Geological and Planetary Sciences

California Institute of Technology, Pasadena, CA 91125

4. Lawrence Livermore National Laboratory

Livermore, CA 94550 USA

5. SWRI, Boulder, CO??

Submitted 21 October 2005 to J. Geophys. Planets, Special Titan Issue on:

Coordinated Earth-Based Observations of Titan During the Huygens Mission.

31 pages; 14 figures; 2 tables.

Abstract

We present adaptive optics data from the 10-m W.M. Keck telescope that were taken during the time the Huygens probe descended through Titan's atmosphere, and on the days following touch-down. The spatial resolution of the images is typically $\sim$0.04″ , or $\sim$ 240 km on Titan (60 km/pixel). No probe entry signal was detected at levels exceeding 0.8 μJy (3-σ) per pixel (0.01"), which although within the range of predicted flux levels, cannot constrain any models.

We present data on Titan's surface, troposphere and stratosphere during the days following probe entry, when the solar phase angle varied from 0.05° up to 0.8°, with the Sun in the West. Contrary to expectation, the data often showed the East side to be brightest. Adding data obtained with Keck and Gemini over the past few years reveals that the East-West asymmetry can be explained by a combination of the solar phase angle effect together with a general preponderance of haze on Titan's East or morning hemisphere.

The troposphere was characterized by quiescent weather; only a few small clouds were present near the south pole, at typical altitudes of 30–40 km. While stratospheric haze was prominent over the northern hemisphere, tropospheric haze dominated the south, from the S. pole up to latitudes of $\sim -45°$. An intriguing observation is that obtained at 1.22 μm, which revealed haze in the form of a collar at $-60°$, in contrast to the polar haze cap as usually seen.

A comparison of narrow band JHK images of Titan's surface with that obtained by Cassini ISS shows a striking resemblance in small-scale features. After a decent attempt to remove the atmosphere from the images, the surface contrast between dark and bright areas may be larger at 2 μm than at 1.6 and 1.3 μm. If true, this could imply that the dark areas on Titan's surface are covered by a coarser grained frost than the bright areas, and/or that there are more absorbers, such as NH_3/NH_4SH frost, in these dark areas.

1. Introduction

On 14 January 2005, at 10:13 UTC, the Huygens probe entered Titan's atmosphere. Almost 2.5 hours later, at 12:34 UTC, it touched down on the satellite's surface where it remained operational for another hour and 12 minutes. The timing and viewing geometry of the event were excellent for observatories on Mauna Kea, Hawaii. We observed Titan with the adaptive optics system on the 10-m Keck telescope to characterize/monitor the weather while the probe did glide down through its atmosphere. Our data form part of a long-term monitoring program of Titan carried out by several groups at different 8–10-m sized telescopes. The data taken near probe entry time are particularly valuable in this dataset because it allows modeling with 'ground-truth' data taken by the probe during its descent (e.g., temperature-pressure profile, winds, hazes, clouds).

In Section 2 we present the observational details, and discuss the deconvolution process used to sharpen some of the images. The probe entry results are evaluated in Section 3. In Section 4 we show a few spectra with retrieved haze profiles. The results are utilized to derive contribution functions for the various filters used to image the satellite. Results pertaining to Titan's atmosphere are discussed in Section 5, and regarding its surface in Section 6.

2. Observations and Data Reduction Techniques

We observed Titan with the 10-m W.M. Keck II telescope on UT 14 – 17 January, 2005, during the time that the Huygens probe made its descent through Titan's atmosphere and on subsequent nights. We used the adaptive optics (AO) system with the facility Near-Infrared Camera NIRC2, which has a 1024 × 1024 Aladdin-3 InSb detector array. We used NIRC2 in high angular resolution mode, 9.94 ± 0.03 mas per pixel (de Pater et al. 2006), which translates to 58.2 km/pixel on Titan. In addition to broad and narrow band imaging, we took low-resolution spectra in H (1.582-1.749 μm) and K' (1.999-2.221 μm) bands at a spectral resolution $R = \lambda/\Delta\lambda \approx 1600 - 1700$, with λ the wavelength. A detailed log of the observations is provided in Table 1. The approximate altitudes probed by the various filters are summarized in Fig. 5, and discussed in Section 4.

All images were processed using standard near-infrared data reduction techniques (flat-fielded, sky-subtracted, with bad pixels replaced by the median of surrounding pixels). We typically obtained a spatial resolution (FWHM) of $\sim$0.05$''$ in K' band, and $\sim$0.04$''$ in J and H band. Strehl ratios [the ratio of the peak intensity of the observed point spread function (PSF) to the theoretical maximum for the telescope aperture] were $\sim 0.35 - 0.50$ in K', ~ 0.4 in H, and $\sim 0.1 - 0.2$ in J band.

Photometric calibrations were performed on the stars HD22686 and HD129655 (Elias et al. 1982). These measurements were used to derive the conversion factors in Table 1, with which to multiply the images (in cts/sec) to convert them to I/F, a dimensionless quantity. I is the intensity reflected by Titan at the wavelength observed, and πF is the solar flux density received by Titan at the same wavelength (Colina et al. 1996a). I/F equals the geometric albedo when viewed at zero phase angle. The observed disk-averaged I/F in each filter is tabulated in Table 1.

In addition to the basic-processed images, we also present images sharpened with a deconvolution algorithm. We used `AIDA`, an Adaptive Image Deconvolution Algorithm (Hom et al. , 2006), which is similar to `MISTRAL`, a Myopic Iterative STep-preserving Restoration ALgorithm, especially aimed at AO observations of planetary objects (Mugnier et al. 2004). `MISTRAL` and `AIDA` use a stochastic approach to find the best image reconstruction, using information both about the object and the PSF. The main improvement in the `AIDA` algorithm to date is its speed and an automatic search for the best regularization parameters (it is about 200 times faster than `MISTRAL`).

To check the reliability of the algorithm, we constructed two simulated images of Titan. We used the Gibbard et al. (1999) model, constructed to simulate Keck images of Titan obtained via speckle interferometry. Model 1 consists of a disk with a surface albedo of $\sim$0.04 and atmosphere with a north-south gradient, and east-west asymmetry. This model is analogous to Titan observed through a stratosphere probing filter, as e.g., FeII or Brγ. Model 2 is more analogous to Titan probed through a broad K-band filter. We added a relatively bright feature on Titan's surface. On both model images, we added Poisson noise (signal to noise is $\sim$150:1, a little worse than in our data) and convolved the model with a PSF (image of an observed star). We deconvolved these models with `AIDA` to address how well surface features and limb brightening characteristics are recovered (see also Marchis et al. 2006 for more deconvolution reality checks, in particular with respect to shape and size of objects).

Results of our deconvolution tests are summarized in Fig. 1. Images are shown in the top panels: *i*) the original images, *ii*) after addition of Poisson noise and convolution with a PSF, and *iii*) the `AIDA` deconvolved maps. All data were normalized to the disk-averaged value of the original images. The lower panels show scans through the images, approximately along the horizontal and vertical lines on the images. The surface feature in Model 2 was easily recovered, as well as the limb brightening east-west and north-south. In Model 1 the limb brightening is very steep, and is recovered only partially via deconvolution. This, however, is not surprising, since structure at spatial scales considerably smaller than the diffraction limit of the telescope (approximately the core of the PSF) cannot be recovered. We further see that the sharp edge of the disk is indeed recovered well, as advertized for these algorithms.

Spectra of Titan were obtained in H and K' bands by stepping the spectrometer slit across Titan. While stepping across the satellite, we shifted Titan up and down along the slit, so the sky would be removed by subtraction of adjacent observations. All data were flatfielded, and bad pixels were replaced by the median of surrounding pixels. Wavelength calibration was based on OH lines from the Earth's atmosphere (Rousselot et al. 2000). In order to correct for telluric absorption and the instrumental transfer function, we observed A and G-type stars. The A stars were divided by the spectrum of Vega (spectral type A0 V; Colina et al. 1996b), and multiplied by a solar blackbody spectrum. The Titan spectra were then divided by the transfer function derived from these spectra. Finally, the spectra were absolutely calibrated using narrow band images that cover a fraction of the spectrum. In particular, we used FeII images to calibrate the H band spectra, and both the $H_{2(\nu=1-0)}$ and Brγ (average scaling factor) to calibrate K' band.

3. Titan During Probe Entry, 14 January 2005

During the time the Huygens probe descended through Titan's atmosphere we took a sequence of 80 images, 10 seconds each, in the CH_4L filter. This filter is ideal for these measurements, since it probes primarily Titan's stratosphere, and yet is broader than the conventional narrow band filters that probe this region (Fig. 5). The observations started at 10^h:01^m:08^s.5 UT, and continued through 10^h:20^m. At that time there was a failure in the adaptive optics system, and we lost the telescope for almost an hour. When it came back we observed Titan in the broad surface probing K' band and the narrow $H_2(\nu = 1-0)$ filter that probes the troposphere.

Time-averaged images of Titan through all three filters are shown in Fig. 2a–c, with the viewing geometry in panel d. We indicate the approximate position of the Huygens probe landing spot on one of the images. Unfortunately, the weather was far from optimal with winds reaching over 35 mph. The quality in these images is therefore lower than usual for this instrument.

Probe entry time (passing the 1270 km altitude in Titan's atmosphere) was at 10^h:13^m UT (all times are referenced to receiving time on Earth). At 10^h:17^m, when the probe was at an altitude of 180 km, the parachute was deployed. One minute later, from an altitude of 160 km, Huygens began to transmit radio signals to the Cassini spacecraft, which were detected on Earth by a network of radio telescopes (Bird et al. 2005). Most of the probe's kinetic energy was expected to be released at altitudes between 400 and 250 km, around 10^h:16^m (Lorenz, 2002; Lorenz et al. 2006). To search for a possible meteorite flash in our stack of 80 CH_4L images, we first subtracted the time-averaged image (Fig. 2c) from each frame. We did not remove cosmic rays or "hot" pixels from the frames, to make sure not to remove any potential meteorite signal. We searched for the peak intensity within a 15×15 pixel box, encompassing the entire probe entry track. Because this night was not particularly photometric, we subtracted the median background from this peak intensity, where the median intensity was calculated over a box twice as large. Under ideal circumstances this intensity is close to zero, since the time-averaged image was already subtracted. The result is shown in Fig. 3, a graph of the peak intensity as a function of time (in minutes after 10:00 UT). The $3-\sigma$ RMS value is 0.8 μJy. Hence, no signal over 0.8 μJy relative to the average background signal of 0.75 μJy has been detected. This signal thus refers to the upper limit of a meteorite flash within a single pixel ($0.01 \times 0.01''$) over a 10 second integration interval.

Lorenz et al. (2006) predicted (in retrospect) that groundbased telescopes at visible and near-infrared wavelengths might detect an intensity of up to 2.7 μJy, a factor $\sim$ 3–4 above our upper limit. However, as pointed out by the authors, a large fraction of the radiation was blocked by the probe itself, so perhaps only $\sim$10% of this radiation could have been detected in reality. Additional uncertainties in the various assumptions (e.g., surface area of heat shield) may cause a further decrease in the predicted flux density. So although our upper limit is close to expected detection limits, it is not good enough to constrain potential entry models.

4. Spectroscopy, Haze Distribution and Contribution Functions

Titan's 3D atmospheric haze distribution can be derived from spectral image data cubes. Ádámkovics et al. (2004) performed such an analysis using Keck AO data obtained in February 2001. We obtained H and K' band image data cubes on Jan. 15–17 (Section 2). Although a full analysis of these data will be presented in a future paper, we show a few spectra here to aid in the analysis of our narrow band images. Figure 4a shows H-band spectra from January 16 at the center of the disk, and at latitudes of 50°N and 80°S, i.e., offset from the center by 0.35″ to the north and south. These spectra show an enhanced flux density from the north in the stratosphere, at wavelengths $\lambda \gtrsim 1.63$ μm. The troposphere is probed at 1.61–1.63 μm. Tropospheric haze is clearly present near the south pole, although at much reduced levels compared to 2001 (see Ádámkovics et al. 2004).

We used Ádámkovics *et al.*'s (2006) model to retrieve haze density profiles, which we use below to determine the altitude range probed in our narrow band filters. This model is essentially an update and extension of the Griffith et al. (1991) model, which was build on McKay *et al.*'s (1989) two-stream code including multiple scattering by aerosols. The optical depth in Titan's atmosphere is dominated by methane gas absorption and scattering by aerosols. To calculate the absorption by methane gas we make use of Irwin *et al.*'s (2005) correlated k-coefficients, and adopt a methane abundance of 5% at the surface, following the saturated vapor curve where appropriate. In the stratosphere we adopt an abundance of 1.6% (Tomasko et al. 2005). We use Lellouch *et al.*'s (1989) temperature-pressure profile. The single scattering albedo was held constant at $\varpi = 0.95$. The asymmetry parameter, g, in the Henyey-Greenstein phase function is usually set at $g = 0.8$, but we have tried different values.

As discussed in detail by Ádámkovics et al. (2006), it is impossible to derive a unique haze density profile from the data. In this paper we show results for two profiles. *i*) We constrain the haze density to decrease exponentially with a 100 km scaleheight in the stratosphere, above ~40 km, and to be constant below that. These assumptions are consistent with the Huygens probe measurements (Tomasko et al. 2005). Independent of particle size/properties, we then determine the haze extinction by fitting the observed spectra, starting in the stratosphere at wavelengths where neither the troposphere nor surface are 'seen' ($\lambda > 1.63$ μm at H, $\lambda > 2.16$ μm at K). Next we optimize the fit at shorter wavelengths by including tropospheric haze and surface albedo. The difference in extinction between H and K band is approximately equal to that expected for Mie scattering by 0.3–0.5 μm sized particles (Ádámkovics et al. , 2006). *ii*) We also find a best fit to the spectrum that is sensitive to the troposphere by partially clearing the haze in this region from the ground up, which physically could be caused by condensation and rainout (McKay et al. 2001, and references therein). For these models the haze extinction follows a 32.5 km scaleheight above 60 km, and is 16.8 km below. The resulting haze density profiles at the center of Titan's disk are shown in Fig. 4b.

These haze profiles are used to determine the approximate altitude range probed in our narrow band filters. We calculate the contribution functions, $C_\lambda(n)$, at each wavelength, λ:

$$C_\lambda(n) = [F_n^u - F_n^l e^{-\tau_n/\mu_n}] \times exp\left(-\sum_{i=n}^{N} \tau_i/\mu_i\right)/F_0 \ . \quad (1)$$

In this equation, F_n^u and F_n^l are the upward fluxes of the upper and lower boundaries of each layer, n, in Titan's atmosphere, with F_0 the flux observed from the top of the atmosphere, at each λ. The first term in eq. 1 is the difference in upward fluxes between the top and the bottom of the layer, decreased exponentially by the optical depth, τ_n, in that layer. The optical depth is scaled by the effective pathlength $1/\mu_n$ ($\mu = \cos\theta$, with θ the angle the line-of-sight makes with the local normal to the disk). In addition, the μ used here has been corrected for the plane-parallel approximation of Titan's atmosphere, as suggested and validated by Tran and Rannou (2004). The entire flux is attenuated by the total optical depth above that layer. The contribution from the surface is given by:

$$C_\lambda(surf) = F_{surf} \times exp\left(-\sum_{i=0}^{N} \tau_i/\mu_i\right)/F_0 \ , \qquad (2)$$

with F_{surf} the flux reflected from the surface at λ. By averaging contribution functions at individual wavelengths over the various filter bandpasses, we obtain the profiles shown in Fig. 5. As expected, these profiles depend on our atmospheric model, in particular the haze density profile.

Both haze profiles (*i* and *ii* above) give good fits to the data. However, there are several shortcomings in the present models that explain why such different haze profiles, and hence contribution functions, are all consistent with the data. These shortcomings are best illustrated by Ádámkovics *et al.*'s (2006) Fig. **. In H band, the model spectrum is too high at wavelengths that probe the troposphere, and at K band the model spectrum 'overshoots' the I/F that might represent the surface. These discrepancies between models and observations are probably caused by excluding weak methane absorption bands in the models, due, in part, to the fact that not all measured transition frequencies have been assigned, and/or the line intensities are not right. The strong bands are properly incorporated in Irwin *et al.*'s (2005) correlated k-coefficients, and allow proper modeling of Titan's stratosphere. Weak absorption bands allow probing Titan's troposphere, while the surface can be probed only if methane absorption is very small. By ignoring weak methane bands, the models are quite insensitive to Titan's troposphere, and may indicate surface reflectivities that are inconsistent with the data. Despite these shortcomings, the two models shown, however, clearly distinguish filters probing the upper stratosphere versus those probing the lower stratosphere/troposphere. Since the models are not very sensitive to the troposphere, the contribution functions are probably best represented by the models in which the troposphere has been cleared, even though the Huygens' data revealed a constant haze density in the troposphere (Tomasko et al. (2005).

5. Titan's Atmosphere

5.1 Stratosphere: East-West Asymmetry

Titan was near opposition at the time of probe entry, so that the solar phase angle, α, changed from 0.05° up to 0.4° during our observations, with the Sun on Titan's West side (right on figures). Note that the Sun really was about 180° away from Titan, though. This timing is ideal to investigate the controversial cause of the observed east-west asymmetries in Titan's atmosphere: are the asymmetries caused by a solar phase angle effect (i.e., induced by the Sun), or by the presence of an enhancement in the haze density on the morning side? Roe et al. (2002a) observed Titan's stratosphere in October 1999, August 2000, and February 2001, at solar phase angles of 0.9° (Sun in the East), 6.3° (Sun in the East), and 6.2° (Sun in the West), respectively. The side facing the Sun was always brightest ($\sim$ 10%). These observations thus confirm east-west asymmetries to be dominated by the solar phase angle effect. The authors, however, could not rule out the presence of a haze enhancement in the morning at small phase angles. The presence of such a haze had been hypothesized by Coustenis et al. (2001), who had observed Titan just past opposition, at $\alpha = 0.5°$, with the Sun in the West; i.e., their viewing geometry was very similar to ours. Like Roe et al. (2002a) they used filters that probe the lower stratosphere, and noticed (after deconvolution) that the east-limb of Titan was brighter than the west-limb, opposite to that expected from the solar phase angle effect. The authors suggested an enhancement in the haze density in the East, which they attributed to condensation at night. They called this enhancement a "morning fog". However, fog is a phenomenon that occurs in the troposphere, usually near the ground, while the haze enhancement on Titan is seen in the stratosphere. We therefore refer to it simply as "haze enhancement", regardless of its origin.

Figure 6 shows images taken through several narrow band filters on 14 – 17 January, complemented with data on January 20 (Table 2). These filters probe different regions in

Titan's atmosphere, as characterized through the contribution functions in Fig. 5. Images in Jcont and Kcont/CO were only obtained on January 15. Fig. 7 shows Jan. 15 images after deconvolution, which sharpened them significantly. The tropospheric cloud features in the south, as well as the limb brightening in all filters is clearly visible. Fig. 8 shows east-west scans through the images in Fig. 6, sorted by filter, and displaced in I/F for clarity. These are horizontal (EW) scans at 15° N latitude. The West (right side = evening) is usually slightly brighter on Jan. 15, while the East (morning) is brightest on Jan. 16–20. In $H_{2\ \nu=1-0}$ the East side is brightest on 14 January, which switches to the West on 15 January, and then back to the East through 20 January. In the CH_4L filter the West side is brighter than the East side on January 14 and 15, while the asymmetry is reversed on January 16 and 17. Similarly, on January 15 the West side is brightest in Brγ and FeII, while the east side is brightest on January 16 – 20.

In the following we use simple models to calculate the variation in the east/west ratio with solar phase angle, and compare the results with data obtained over the past few years with the 10-m W.M. Keck and 8-m Gemini telescopes. We evaluate the effect on the east/west ratio of *i*) Titan's shadow, *ii*) extinction of the radiation, *iii*) scattering by aerosols, and *iv*) combined extinction and scattering in Titan's atmosphere.

i) To investigate the effect of Titan's shadow on the observations, we built a simple model of a satellite with an atmosphere extending up to 500 km above its surface. We assumed that each volume element along the line-of-sight contributes equally to the observed brightness, unless it is in Titan's shadow, when we assign the volume element a zero brightness (see Fig. 9 for a sketch of the geometry). We note that this model [in *i*) and *ii*)] includes Titan's full spherical geometry, and does not depend on the assumption of a plane parallel atmosphere. These calculations are in essence for an optically thin single scattering atmosphere without extinction. The ratio between the morning and evening (called sunlit and 'dark' hereafter) limbs is shown by the dashed curve in Fig. 10, for model images with a resolution of $0.04''$. A lower (higher) resolution would decrease (increase) the EW asymmetry. At $\alpha < 0.5°$ there is no phase angle effect; at $\alpha = 1°$ the effect is only 1%. The asymmetry becomes noticeable only at larger phase angles, when a larger fraction of the atmosphere is shadowed by Titan.

ii) Titan's atmosphere is far from optically thin, and solar rays will be attenuated more on the dark side, where the pathlength through the atmosphere is larger (Fig. 9). As in *i*), we model Titan's atmosphere up to 500 km above its surface, and adopt a characteristic extinction profile as retrieved from spectra (Fig. 4). We calculate the effect for 4 different filters: Kcont, $H_{2(\nu=1-0)}$, Brγ and FeII. As expected, the east-west asymmetries for the three stratosphere probing filters are very similar (one curve shown), while the deeper probing filter ($H_{2(\nu=1-0)}$) shows a slightly lower sunlit/dark ratio (note that at the limb this filter probes the lower stratosphere rather than troposhere). Although the shadow effect was taken into account in these calculations, its effect is essentially zero due to the relatively high extinction coefficients.

iii) We see Titan's atmosphere since aerosols scatter incoming sunlight. To evaluate the effect a change in illumination angle would have on a scattering atmosphere, we made use of van de Hulst's (1980) Table 12. This table is constructed for a finite plane-parallel atmosphere, viewed and illuminated under different directions. To estimate the sunlit/dark ratio near the limb of Titan, we choose $\theta = 60°$. As shown in Fig. 9, $\theta_0 > \theta$ on the dark, and $\theta_0 < \theta$ on the sunlit side. We find that the sunlit/dark ratio for an isotropically scattering atmosphere with total optical depth $\tau = 2$, and single scattering albedo, $\varpi = 0.20$ is essentially equal to the extinction-only curve for the stratosphere. The top dashed line in Fig. 10 is for a plane-parallel atmosphere with $\tau = 2$ and $\varpi = 0.60$. The sunlit/dark ratios increase if the aerosols become more reflective (increase in ϖ) and/or the haze density increases (increase in τ). If the scattering phase function is changed to a Henyey-Greenstein phase function with asymmetry factor $g > 0$, the ratios are smaller (Table 27 in van de Hulst, 1980). Although these calculations were performed for a plane parallel atmosphere, we find the results enlightening for our discussion of EW asymmetries.

iv) Gibbard et al. (1999, 2004) used a plane parallel radiative transfer model to simulate the absorption, reflection and multiple scattering of photons from Titan's atmosphere and surface (constant albedo), assuming longitudinal symmetry, and a smooth variation in haze density with latitude. Their model uses 10 layers in altitude, with the haze confined to the upper layers and methane underneath. The model includes the correction factor of Tran and Rannou (2004) to properly model Titan's limb. We used this model with the haze parameters as determined by Gibbard et al. (1999) to evaluate the variation with solar phase angle. We obtained results very similar to the stratospheric extinction-only model in Fig. 10.

Our calculations in $i) - iv)$ show that the east-west asymmetry should increase approximately linearly with α, up to $\sim 20\%$ at $\alpha \approx 6^\circ$ for spatial resolutions of $\sim$0.04″.

Observations are shown in Fig. 11. We supplemented our data with Keck AO images at larger phase angles, as tabulated in Table 2. We determined the East/West ratio on each image simply by dividing the peak intensities on the east and west limbs, along a horizontal scan through the center of the image. The 3 central rows were averaged to improve the signal to noise. For the 2001 data we averaged the central 5 rows. The uncertainty was derived from the standard deviation near the center of the disk. The East/West ratio is plotted as a function of solar phase angle, where we define $\alpha > 0^\circ$ when the Sun is in the East, and $\alpha < 0^\circ$ when the Sun is in the West. The solid line shows the Gibbard model, discussed in *iv*) above. Clearly, most data points lie above the line, indicative of an overall enhancement in haze density on the East or morning side. The dashed line is for a model where the haze density on the east side was arbitrarily increased by 10%.

Roe et al. (2005) initiated an intensive observing program at the 8-m Gemini telescope in November 2003, a program that is still ongoing. The observations have been obtained with the NIRI camera coupled to the adaptive optics system (Hodapp et al. 2003), which has a pixel size of 0.022″/pixel. These observations span the full range of solar phase angles. Since the spatial resolution is lower than at Keck, we show the Gemini data by themselves in Fig. 11b, with overplotted the same Gibbard models but convolved down to a resolution of 0.10″. These data show the same phenomenon as those in Fig. 11a: Most data lie above the solid line, and clearly suggest a several percent enhancement in the haze density on the morning limb.

For both telescopes we showed E/W ratios for different parts in the stratosphere (primarily $H_{2(\nu=1-0)}$ and Brγ filters). Although on individual days the ratios measured in the two filters are sometimes noticeably different, we do not see a specific trend between ratios measured in the lower versus upper stratosphere. As mentioned above (Fig. 6), there may be asymmetry reversals between images taken through different filters on the same day (e.g., at $\alpha = 0.05°$ and $1.13°$), and sometimes larger than average day-to-day variations. From the entire collection of data we conclude: *i*) The E/W ratio is strongly influenced by the solar phase angle effect. *ii*) The haze tends to be enhanced on the morning side, by up to $\gtrsim 10\%$. *iii*) No clear correlation in E/W asymmetry with altitude has been detected. *iv*) There is a suggestion of additional azimuthal inhomogeneities in the haze density. We do need to add a cautionary note here, though. The E/W ratio is strongly affected by the Strehl ratio of the observations. A low ratio tends to equalize the intensities at the limb of the satellite. Variations in Strehl ratio are the most likely cause of the mean spread in the data, and of E/W ratios that are closer to unity compared to expectations. E/W ratios that are exceptionally large (in absolute sense) are harder to attribute to observational problems, although an apparent motion of the object on the sky (due e.g., to high winds, or starting the integration before the system was completely ready) could influence the EW ratio. Usually such effects are obvious in the data, and such points were removed prior to plotting.

At this time we cannot give a full explanation for the haze enhancement effect. When Coustenis et al. (2001) first suggested this effect on Titan's morning side, they suggested possible enhanced condensation at night. Indeed, a parcel of air will spend at least a terrestrial day on the night side of Titan, considering that zonal winds usually do not exceed velocities of $\sim$ 100–150 m/s (e.g., Moreno et al. 2005; Bird et al. 2005). If the stratosphere is colder at night then during the day, species may condense out. Whether there is a temperature drop at night, however, remains ambiguous (Lindal et al. 1983; Coustenis et al. 2001). Regarding possible changes in the EW asymmetry over time, and/or anticorrelations between altitudes, we note that the Cassini spacecraft observed variations in Titan's haze layers over time scales of hours (Porco et al. 2005). Since the windshear in Titan's stratosphere is strong (Bird et al. 2005), vertical mixing between layers may be small. In addition, cryovolcanism or geysers may supply the atmosphere episodically (Roe et al. 2005), although in our data we do not see any correlation in the EW asymmetry with Titan longitude. This may not be surprising, since we probe well above the tropopause, and vertical mixing between the troposphere and upper stratosphere is not expected.

5.2 Troposphere: Clouds and Hazes

As shown in Figs. 6 and 7, weather on Titan during probe entry and on subsequent days was very quiet. Clouds are most easily spotted in the $H_{2(\nu=1-0)}$ filter (Fig. 5; and Roe et al. 2002b). A small brightening is visible on 14 January in the south, on the morning hemisphere, which is probably caused by a slight enhancement in the local haze concentration. The next day two small features have appeared near the south pole, which become more noticeable on subsequent nights. The quiescent weather may either be fortuitous, or mark a change in weather conditions after the extreme storms in October 2004, as discussed by Schaller et al. (2005). In Fig. 12 we show a set of K' band spectra that were taken on and off a small cloud in the south, on 17 January, as indicated by the arrows on the inset — an AIDA deconvolved image in the narrow band $H_{2(\nu=1-0)}$ filter. The two spectra were taken through the same airmass on Titan. We could best fit the spectra with a cloud at an approximate altitude of 30–40 km, which is similar to the mid-latitude clouds observed by Cassini (Griffith et al. 2005).

The tropospheric haze in the south is clearly visible in both the $H_{2(\nu=1-0)}$ and Jcont filters, while in both filters the northern hemisphere is dominated by stratospheric haze. In the Jcont filter approximately 20% of the reflected light can be attributed to surface reflectivity near the center of the planet, where the optical depth through the atmosphere is smallest. The tropospheric haze in the south as seen in the $H_{2(\nu=1-0)}$ filter covers the south polar region down to a latitude of $\sim -45°$ S, consistent with the findings by Roe et al. (2002b) from images taken in December 2001. At that time, however, there was much more haze near Titan's south pole than at present (Ádámkovics et al. 2006). While the former enhancement may have been caused by sedimentation from higher altitudes, from the time stratospheric haze was still prevalent above the south pole, the more recent measurements may reveal the low latitude return flow in general circulation models (e.g., Rannou et al. 2002) from the north to the south pole.

In the Jcont filter the tropospheric structure is markedly different from that in the $H_{2(\nu=1-0)}$ filter (Fig. 7), being more like a polar collar than polar cap, centered at a latitude of $-60°$ S. This is quite intriguing and begs for a more in-depth multi-wavelength study in the future. The difference in structure between wavelengths may be caused by a wavelength dependence in aerosol scattering.

6. Images of Titan's Surface during Probe Entry

Titan's surface is seen in all three broad band filters J, H, and K', but in all three filters there is a significant atmospheric contribution as well. Several of our narrow band filters probe Titan's surface without much contamination by the atmosphere (Fig. 5). We show the narrow band surface images from 15 January UT in Fig. 13, panels a–c, with deconvolved images in panels d–f. As shown, the deconvolution sharpened the images considerably, although all details are also visible on the original images. We note in particular the improvement in the J band image. The original image is rather blurry because of the low Strehl ratio, and hence large PSF halo. `AIDA`, which solves simultaneously for the best characterization of the object and its PSF, uncovered Titan's fine structure extremely well, as shown. There is excellent agreement in surface structure between the 3 wavelengths, as well as with the Cassini VIMS composite image from the close flyby on 26 October 2004 (panel g), under almost the same viewing angle. In panels *h* and *i* we highlight some of the similarities. Note that in October a bright cloud complex was seen near Titan's south pole, which was absent in January. [*** or change to same viewing aspect, with Mate's program??]

Although the images at the three wavelengths look very much alike, interpretation of surface properties, as composition and structure, make it necessary to quantitatively determine the surface albedo and relative contrast between the bright and dark regions at the three wavelengths. If the atmospheric contribution would be zero, one would simply measure the surface albedo directly, and by dividing images one would see how the relative contrast between bright and dark regions would vary between the 3 wavelengths. However, the atmospheric contribution is not zero, and moreover increases with decreasing wavelength. A simple ratio of maps therefore reveals the same dark/bright pattern (Fig. 14a) as in the original images, as if the contrast between dark and bright areas is largest at 2.06 μm, and smallest at 1.29 μm.

Using Hubble Space telescope (HST) data, Smith et al. (1996) subtracted images of Titan's atmosphere from broadband data to investigate relative albedo variations across the satellite's surface. In analogy, we subtracted the Jcont image from all three narrow band images, weighted by the relative atmospheric contribution in each filter (Figs. 5a, b; 14% at 2.06 μm, 28% at 1.58 μm, and 43% at 1.29 μm). This process will not reveal the absolute surface reflectivities, but may retain the proper contrast. After normalizing the resulting images (so each image I/F equals unity on average), we ratioed them to one another; results are shown in Figs. 14b and c. Interestingly enough, the dark/bright contrast as seen in panel a is still clearly visible, although, as expected, at a reduced level. Hence, the contrast between dark and bright areas may indeed be larger at 2.06 μm than at H or J band (by up to 10–15%). Similar results were obtained after subtracting uniform and Minnaert limb-darkened haze layers at different I/F values from the images.

Ideally, the surface reflectivity and relative contrast between dark and bright areas should be extracted by fitting a full atmosphere–surface coupled model to 3D image data cubes. Ádámkovics et al. (2006) did this experiment using integral-field spectrometer data from the VLT (Sinfoni instrument), obtained simultaneously at H and K bands. Their Fig. ** shows retrieved surface albedos at 5 different locations on Titan's disk. A comparison between models and spectra clearly shows that the models are not optimal (yet). Discrepancies can be attributed to the fact that weak methane absorption bands were not incoporated in the model (Section 4). We therefore think that surface reflectivities derived from models that fit Titan spectra may not (yet) be accurate enough to extract detailed information on surface composition and structure. We therefore used the method of subtracting an image of the atmosphere from our surface data to evaluate the brightness contrast between the 3 wavelengths.

Since our narrow band JHK images probe Titan's surface in H_2O-ice absorption bands, our finding of an enhanced dark/bright contrast at 2.06 μm (if confirmed; note the caveats above) suggests a difference in the absorption characteristics of the water-ice component between the dark and bright areas. Such differences can be caused by the shear amount of ice, the temperature of the ice, the grain size of frost and whether or not the frost is coating a layer of solid ice. Since low albedo features absorb more sunlight, they will be warmer than their bright counterparts. A difference in albedo of 10–20% will only induce a temperature difference of 3–6 K. This leads to changes in absorptivity over our bandwidths of no more than 1–2% (Grundy and Smitt, 1998). Hence, the difference in surface contrast between the various wavelengths cannot be explained by a difference in surface temperature between the dark and bright areas.

Absorption spectra of water ice change dramatically with grain size and whether or not one probes down to a layer of solid ice. We probably can discard the latter scenario, based upon measurements of the dielectric constant by Elachi et al. (2005). They determined a bulk dielectric constant of 2, which is inconsistent with that of solid water ice (3.1), or ammonia ice (4.5), but would be consistent with porous ice and/or an organic sludge. If the frost is fine-grained, scattering predominates and will subdue weak absorption features, in contrast to coarse grained frost, where absorption dominates (e.g., Fink and Sill, 1982). Perhaps water ice on the bright terrain consists of a finer grained frost than the ice on Titan's dark terrain, which would lead to a relative decrease in the 1.6 μm absorption feature compared to that at 2.0 μm (Clark, 1980). Such a difference in grain size could be caused by a dark terrain that is, or has been, 'wetter' (hydrocarbon slush) in the past. Alternatively, or in addition, it is also feasible that there are additional absorbers in the dark terrain, such as NH_3 and/or NH_4SH frost, which absorb more at 2 than at 1.6 μm(Fink and Sill, 1982). Ammonia is expected to be present in some form, since it was probably present in the form of ammonia hydrates when the satellite formed, a leading theory to explain the formation of Titan's nitrogen atmosphere (Lewis, 1971; Waite et al. 2005). Since ammonia lowers the freezing temperature of water considerably, its presence would also readily explain cryovolcanism on Titan.

7. Conclusions and the Future for Groundbased Observations

We presented Keck AO data in the form of spectra and narrow band images that were taken during the time the Huygens probe descended through Titan's atmosphere, and on the days following touch-down. The spatial resolution of the images was near the diffraction limit of the telescope, $\sim$0.04$''$ ($\approx$ 240 km on Titan). No meteorite trail was detected in the data. The atmosphere was relatively clear during probe entry time and on the following days, except for a few small clouds near the south pole, at typical altitudes of 30–40 km. Haze was prominent above the northern hemisphere in the stratosphere, while tropospheric haze was present in the south, shown both in the $H_{2(\nu=1-0)}$ and Jcont filters. In the latter filter the haze was distributed in the form of a collar at $-60°$. Although the haze is clearly visible in the images, it is much less intense than in 2001. Perhaps we now see the haze resulting from the low altitude return flow in general circulation models (e.g., Rannou et al. 2002), whereas in 2001 most of the haze in this region might have resulted from a slow settling of aerosols from above, from the time the stratospheric haze was still present over the south pole.

Our images of Titan's atmosphere clearly revealed an east-west asymmetry that is not a simple function of solar phase angle. To examine this in detail, we extended our database with images at other phase angles, obtained both with Keck and the Gemini telescopes over the past years. We found a clear dependence in the east-west asymmetry with solar phase angle, but noticed that the haze is usually enhanced on the East side, by up to $\gtrsim 10\%$, an observation that supports Coustenis et al. (2001) hypothesis of an enhancement in haze density due to condensation at night. There may also be azimuthal inhomogeneities in the haze distribution, which sometimes favor the West, other times the East side.

Narrow band images of Titan's surface revealed most of the fine structure seen on Cassini VIMS images, in particular after deconvolution with `AIDA`. After correcting the images to first order for Titan's atmosphere, the images suggest that the dark/bright surface contrast at 2 μm is larger than that at 1.6 and 1.3 μm, which suggests that the dark areas on Titan's surface may be covered by a coarser grained frost than the bright areas, and/or that there is more NH_3/NH_4SH frost present in these dark areas.

Future: Continued groundbased observations play a crucial role in the ultimate understanding of Titan's meteorology. We still do not have a good understanding of the mechanisms for formation, evolution and loss of haze particles, nor the significance of how aerosols contribute to the global atmospheric circulation. To develop good models for this, we need to know, for example, the time-dependent spatial and vertical distribution of Titan's haze; i.e., we need to observe this 3-dimensional distribution over at least a full Titan year, or more than 30 Earth years. Such long programs can only be carried out with groundbased telescopes, since space missions are usually too limited in extent. At present the Cassini mission will be in orbit for only $\sim$ 1.5 Titan months, and the Huygens probe sampled just one moment in Titan's history, at one location. Hence, to complement and extend the Cassini/Huygens mission we encourage groundbased observers to continue to observe. Moreover, with recent advances in detector technology, such as the field-integral spectrometers Sinfoni on the VLT and Osiris on Keck, we can now obtain image data cubes of the satellite in just minutes of time, and convert these into 3D haze profiles.

Neither groundbased data nor the Cassini/Huygens mission have identified liquid hydrocarbons on Titan's surface, although the surface topology clearly hints at the presence of liquids in the past. The closest one came to sample liquids was perhaps the observation by the probe penetrometer, which revealed a soft wet subsurface (Zarnecki et al. 2005). The presence of methane gas in Titan's atmosphere requires an efficient recycling mechanism, akin either to the hydrological cycle on Earth or perhaps via active cryovolcanism or geysers. The answer to this question is still outstanding. Lorenz et al. (2005) remarked that rainstorms on Titan are rare, but perhaps extremely violent. Will we ever witnesss such storms? Only time can tell.

In contrast to expectations, the Cassini radar/radio observations determined that the dielectric constant of Titan's (sub)surface layers was inconsistent with water and/or ammonia ice, although can be explained by the presence of porous ice and/or organics. For most objects we have some clue as to composition based upon reflectance spectroscopy. Spectroscopic observations of Titan's surface, however, are challenging since the surface can only be probed in specific windows (outside methane absorption bands), and even in these windows one measures a combination of atmosphere and surface. Revealing surface composition thus requires one to model Titan's atmosphere and surface simultaneously, ideally with data at high spatial and (at least) moderate spectral resolution, such as can be obtained via field-integral spectroscopy over many wavelengths. This clearly is the next step in groundbased Titan research, and will complement and extend the Cassini/Huygens mission.

Acknowledgements

This work was funded through grant AST-0205893 from the National Science Foundation, NNG05GH63G from NASA, by the National Science Foundation and Technology Center for Adaptive Optics, managed by the University of California at Santa Cruz under cooperative agreement No. AST-9876783, and by the the Center for Integrative Planetary Science at the University of California in Berkeley. The data presented in this paper were obtained at the W. M. Keck Observatory, which is operated as a scientific partnership among the California Institute of Technology, the University of California and the National Aeronautics and Space Administration. The Observatory was made possible by the generous financial support of the W. M. Keck Foundation.

The authors wish to recognize and acknowledge the very significant cultural role and reverence that the summit of Mauna Kea has always had within the indigenous Hawaiian community. We are most fortunate to have the opportunity to conduct observations of Uranus from this Hawaiian volcano.

This work was performed under the auspices of the U.S. Department of Energy by University of California, Lawrence Livermore National Laboratory under Contract W-7405-Eng-48.

References

Ádámkovics, M., I. de Pater, H. Roe, S. Gibbard, and C. Griffith, 2004. Spatially-resolved spectroscopy at 1.6 μm of Titan's atmosphere and surface. *Geophys. Res. Lett.*, *31*, L17S05, doi:10.1029/2004GL019929.

Ádámkovics, M., I. de Pater, F. Eisenhauer, M. Hartung, R. Genzel, and C. Griffith, 2006. The 3-dimensional distribution of Titan haze from near-infrared integral field spectroscopy. *J. Geophys. Res.*, this issue.

Bird, M.K., + 14 co-authors, 2005. The vertical profile of winds on Titan. *Nature, 438*, 800-802.

Clark, R.N. 1980. Ganymede, Europa, Callisto, and Saturn's rings - Compositional analysis from reflectance spectroscopy. *Icarus, 44*, 388-409.

Coustenis, A., E. Gendron, O. Lai, J-P. Véran, J. Woillez, M. Combes, L. Vapillon,T. Fusco, L. Mugnier, P. Rannou, 2001. Images of Titan at 1.3 and 1.6 μm with Adaptive Optics at the CFHT. *Icarus*, *154*, 501-515.

Colina, L., Bohlin, R.C., Castelli, F., 1996a. The 0.12-2.5 micron absolute lux distribution of the sun for comparison with solar analog star. *Astron. J., 112*, 307-315.

Colina, L., R.C. Bohlin, and F. Castelli, 1996b. Instrument Science Report OSG-CAL-96-01.

de Pater, I., S.G. Gibbard and H.B. Hammel, 2006. Evolution of the dusty rings of Uranus. *Icarus*, *180*, p. 186-200.

Elachi, C., + 34 co-authors, 2005. Cassini Radar Views the Surface of Titan. *Science, 308*, 970-974.

Elias, J.H., Frogel, J.A., Matthews, K., and Neugebauer, G., 1982. Infrared standard stars. *Astron. J., 87*, 1029-1034.

Fink,U., and G.T. Sill, 1082. The infrared and spectral properties of frozen volatiles, in *Comets*. Ed. L.L. Wilkening. pp. 164-202. Univ. of Arizona Press, Tucson.

Gibbard, S.G., B. Macintosh, D. Gavel, C.E. Max, I. de Pater, A.M. Ghez, E.F. Young, and C.P. McKay, 1999, Titan: High resolution speckle images from the Keck telescope, *Icarus*, *139*, 189-201.

Gibbard, S.G., B. Macintosh, D. Gavel, C.E. Max, I. de Pater, H. Roe, A.M. Ghez, E.F. Young and C.P. McKay, 2004. Speckle imaging of Titan at 2 microns: surface albedo, haze optical depth, and tropospheric clouds 1996-1998. *Icarus*, *169*, 429-439.

Griffith, C.A., T. Owen, and R. Wagener. 1991. Titan's surface and troposphere, investigated with ground-based near-infrared observations. *Icarus*, *93*, 362–378.

Griffith, C.A., + 26 co-authors, 2005. The evolution of Titan's mid-latitude clouds. *Science, 310*, 474-477.

Grundy, W.M., and Schmitt, B., 1998. The temperature-dependent near-infrared absorption spectrum of hexagonal H_2O ice. *J. Geophys. Res., 103*, 25,809-25,822.

Hodapp, K.W., + 13 co-authors, 2003. The Gemini Near-Infrared Imager (NIRI). *Pub. Astron. Soc. Pac., 115*, 1388.

Hom, E.F.Y., F. Marchis, T.K. Lee, S. Haase, D.A. Agard, J.W. Sedat, 2006. AIDA: An Adaptive Image Deconvolution Algorithm with Application to Multi-frame and 3D data. JOSA, submitted.

Irwin, P. G. J., K. Sihra, N. Bowles, F.W. Taylor, S.B. Calcutt, 2005. Methane absorption in the atmosphere of Jupiter from 1800 to 9500 cm^{-1} and implications for vertical cloud structure. *Icarus, 176*, 255-271.

Lellouch, E., A. Coustenis, D. gautier, F. Raulin, N. Dubouloz, and C. Frere, 1989. Titan's atmosphere and hypothesized ocean - A reanalysis of the Voyager 1 radio-occultation and IRIS 7.7-micron data. *Icarus, 79*, 328-249.

Lindal, G. F., Wood, G. E., Hotz, H. B., Sweetnam, D. N., Eshleman, V. R., Tyler, G. L., 1983. The atmosphere of Titan - an analysis of the Voyager 1 radio occultation measurements. *Icarus, 53*, 348-363.

Lewis, J.S., 1971. Satellites of the outer planetrs: Their physical and chemical nature. *Icarus, 15*, 174-185.

Lorenz, R.D., 2002. Huygens Probe: An artificial meteor on Titan? *Astron. Geophys., 43*, 5.14-5.18.

Lorenz, R. D., Griffith, C. A., Lunine, J. I., McKay, C. P., Renno, N. O., 2005. Convective plumes and the scarcity of Titan's clouds. *Geophys. Res. Lett., 32*, CiteID L01201.

Lorenz, R.D., O. Witasse, J.-P. Lebreton, I. de Pater, F. Mazoue, H. Roe, 2006. Huygens Entry Emission: Observations campaign, results, and lessons learned. *J. Geophys. Res.*, This issue.

Marchis, F., M. Kaasalainen, E.F.Y. Hom, J. Berthier, J. Enriquez, D. Hestroffer, D. Le Mignant, and I. de Pater, 2006. Shape, Size and Multiplicity of Main-belt asteroids. I. Keck Adaptive Optics Survey, *Icarus*, in revision.

McKay, C.P., J.B. Pollack, and R. Courtin. 1989. The thermal structure of Titan's atmosphere. *Icarus, 80*, 23-53.

McKay, C.P., A. Coustenis, R.E. Samuelson, M.T. Lemmon, R.D. Lorenz, M. Cabane, P. Rannou, P. Drossart, 2001. Physical properties of the organic aerosols and clouds on Titan. *Planet. Space Sci.*, *49*, 79-99.

Moreno, R., A. Marten, and T. Hidayat, T., 2005. Interferometric measurements of zonal winds on Titan. *Astron. Astroph., 437*, 319-328.

Mugnier, L. M., T. Fusco, J.-M. Conan, 2004. MISTRAL: a myopic edge-preserving image restoration method, with application to astronomical adaptive-optics-corrected long-exposure images. *Optical Soc. America J., 21*, 1841-1854.

Porco, C.C, + 35 co-authors, 2005. Imaging of Titan from the Cassini spacecraft. *Nature, 434*, 159-168 .

Rannou, P., F. Hourdin, and C.P. McKay, 2002. A wind origin for Titan's haze structure. *Nature, 418*, 853-856.

Roe, H.G., I. de Pater, B. A. Macintosh, S. G. Gibbard, C. E. Max, and C. P. McKay, 2002a. Titan's Atmosphere in Late Southern Spring Observed with Adaptive Optics on the W. M. Keck II 10-Meter Telescope, *Icarus Note, 157*, 254-258.

Roe, H.G., I. de Pater, B.A. Macintosh, and C.P. McKay, 2002b. Titan's clouds from Gemini and Keck adaptive optics imaging. *Astrophys. J., 581*, 1399-1406.

Roe, H.G., Brown, M.E., Schaller, E.L., Bouchez, A.H., Trujillo, C.A., 2005. Geographic control of Titan's mid-latitude clouds, *Science, 310*, 477-479.

Rousselot, P., Lidman, C., Cuby, J.-G., Moreels, G., Monnet, G., 2000. Night-sky spectral atlas of OH emission lines in the near-infrared. *Astron. Astrophys., 354*, 1134-1150

Schaller, E.L., M.E. Brown, H.G. Roe, A.H. Bouchez, C.A. Trujillo, 2005. "Dissipation of Titan's South Polar Clouds," *Icarus.* submitted

Smith, P.H., M.T. Lemmon, R.D. Lorenz, L.A. Sormovksy, J.J. Caldwell and M.D. Allison. 1996. Titan's surface, revealed by HST imaging. *Icarus, 119*, 336-349.

Tomasko, M.G., + 39 co-authors, 2005. Rain, winds and haze during the Huygens probe's descent to Titan's surface. *Nature, 438*, 765-778.

Tran, T. T., and P. Rannou, 2004. Comparing 3D spherical Monte-Carlo and 2-stream parallel plane simulation of far-field backscattering image of Titan. Notes du ple du plantologie de l'Institut Pierre Simon Laplace, 2, 18-38.

Van de Hulst, H.C., 1980. *Multiple light scattering. Tables, formulas and applications.* Vols. 1 and 2. New York: Academic Press, 1980.

Waite, J.H., + 20 co-authors, 2005. Ion Neutral Mass Spectrometer Results from the First Flyby of Titan. *Science, 308*, 982-986

Zarnecki, J. C., + 25 co-athors, 2005. A soft solid surface on Titan as revealed by the Huygens Surface Science Package. *Nature, 438*, 792-795.

Figure Captions

Fig. 1. Test rsults of deconvolving artificial Titan images with `AIDA`. At the top we show the original image (left), after adding Poisson noise and convolution with a PSF (middle), and the `AIDA` deconvolved image (right). The lower panels show east-west and north-south scans through these models, approximately along the vertical and horizontal lines on the images.

Fig. 2. Images of a): Titan's surface (K' band), b): troposphere ($H_{2(\nu=1-0)}$, and c): stratosphere (CH_4L) during the time the Huygens probed descended through Titan's atmosphere. The approximate landing site of the probe is indicated by the arrow. The viewing geometry is shown in panel d. The latitude and longitude lines are drawn every 15°.

Fig. 3. Timeseries of peak intensities in CH_4L images near the probe entry site. No 'meteorite' trail is visible above a $3-\sigma$ of 0.8 μJy above the avergae background of 0.75 μJy. Probe entry time (passing the 1270 km altitude in Titan's atmosphere) was at 10^h:13^m UT. At 10^h:17^m the probe passed an altitude of 180 km.

Fig. 4. a): Spectra at 3 locations on Titan's disk, along the meridian: at the center (latitude 23° S), in the north ($50^c irc$ N), and in the south (80° S). b) Haze density profiles retrieved from the spectra in panel a, using either the tropospheric clearing model or a model with a constant haze profile in the troposphere (solid lines), in analogy with the Huygens probe findings (dashed line).

Fig. 5. Contribution functions for the various narrow band filters used in this paper. We adopted the atmospheric haze profile that best fits the H band spectral data (Fig. 4b).

Fig. 6. Timeseries of images through different narrow band filters that probe Titan's atmosphere. The UT date and filter is indicated for each image.

Fig. 7. Images from January 15 after deconvolution with AIDA.

Fig. 8. East-west (horizontal) scans through all images from Fig. 6. The scans were taken at a latitude of $\sim 15^\circ$ N (on the central meridian).

Fig. 9. Sketch of the geometry for the calculations in Fig. 10. We look down on Titan's orbital plane. The direction to the Sun and the observer, and the angles θ (to the observer) and θ_0 (to the Sun) on both the sunlit and dark side are indicated.

Fig. 10. Various model results to assess the east-west asymmetry (sunlit/dark side) on Titan as induced by a solar phase angle effect. Full details are given in the text. The dotted blue line (lowest curve) is for a model where only shadowing was considered (atmospheric opacity ignored). The black dashed and red solid lines are models where only extinction in the atmosphere was taken into account. The lower graph is for a filter probing the troposphere/lower stratosphere, while the upper graph is for the stratosphere. The extinction profile as a function of altitude was taken from the best fit parameters of the Titan H band image data cube (Fig. 4). The top (dot-dash cyan curve) line is for a plane parallel atmosphere with isotropic scattering, and a single scattering coefficient $\varpi = 0.60$. Details are given in the text.

Fig. 11. Observations of the east-west asymmetry on Titan as a function of solar phase angle. In panel a we show results based on Keck images (see Tables 1 and 2), and in panel b from Gemini data (from Roe et al. 2005). The solar phase angle was defined positive for the Sun in the East, and negative for the Sun in the West. Superposed is the Gibbard et al. (1999) model as discussed in the text. The solid line is for a haze distribution that is homogeneous in longitude, and the dashed line for hazes enhanced by 10% on the east side.

Fig. 12. K-band spectra from 17 January 2005, taken on and off a cloud feature, at the same Titan airmass. The inset is a `AIDA` deconvolved image in the narrow band $H_2(v = 1-0)$ filter. The clouds are clearly visible on this image.

Fig. 13. Titan's surface viewed through several narrow band filters on January 15 (Paβ, Hcont and He1B) at a central meridian longitude CML = 177°. The top row shows the basic processed images from January 15; the middle row shows the same data after AIDA deconvolution. In panel g we show a Cassini image taken with the Narrow Angle Camera of the Imaging Science Subsystem at 0.9 μm, taken during Cassini's close approach on 26 October 2004 at a CML = 156°. This mosaic of Titan's surface was made from 16 images (NASA/JPL/Space Science Institute). Panels *h* and *i* highlight similarities between the Cassini and Keck images.

Fig. 14. Ratioed images: a) He1B/Hcont from Fig. 13a and b (see text for discussion). b) He1B/Hcont after removal of the atmosphere, as discussed in the text. c) Hcont/Paβ after removal of the atmosphere.

Table 1. Log of Titan Observations in January 2005

UT Time[1] day-hr:min[1]	I/S[2]	Filter	Wavelength range μm	# frames[3] $\times$ sec	CML[4] °	Phase angle[5] °	Calibration[6] Factor $\rightarrow I/F$	Titan's I/F
14-09:59	I	CH_4L	1.613 - 1.749	80 x 10	156.6	0.047	9.67 e-5	0.015
14-11:16	I	K'	1.948 - 2.299	4 x 10	157.8	0.054	7.50e-5	0.033
14-11:28	I	$H_2(\nu = 1 - 0)$	2.111 - 2.145	4 x 30	158.0	0.055	1.0e-3[7]	0.023
15-07:00	I	K'	1.948 - 2.299	4 x 30	176.5	0.154	8.07e-5	0.024
15-07:30	I	J	1.166 - 1.330	3 x 30	176.9	0.156	6.57e-5	0.053
15-07:36	I	$H_2(\nu = 1 - 0)$	2.111 - 2.145	3 x 60	177.0	0.157	1.37e-3	0.0237
15-07:43	I	H	1.485 - 1.781	3 x 30	177.1	0.157	4.19e-5	0.028
15-07:48	I	HeIB	2.040 - 2.072	3 x 60	177.2	0.158	1.26e-3	0.0643
15-07:53	I	Brγ	2.152 - 2.185	3 x 60	177.3	0.158	1.44e-3	0.0120
15-07:58	I	CH_4L	1.613 - 1.749	3 x 30	177.4	0.159	1.02E-4	0.0125
15-08:03	I	FeII	1.633 - 1.658	3 x 60	177.5	0.159	5.52e-4	0.01320
15-08:08	I	Hcont	1.569 - 1.592	3 x 30	177.6	0.159	1.41e-3	0.171
15-08:13	I	Paβ	1.281 - 1.300	3 x 30	177.6	0.160	1.33e-3	0.259
15-08:17	I	Jcont	1.203 - 1.233	3 x 30	177.7	0.160	1.56e-3	0.0955
15-08:22	I	Kcont	2.256 - 2.285	3 x 60	177.7	0.161	2.34e-3	0.0069
15-08:28	I	$CO_{\nu=2-0}$	2.276 - 2.302	3 x 60	177.9	0.161	2.87e-3	0.0065
15-09:37	I	K'	1.948 - 2.299	25 x 5	178.9	0.167	8.07e-5	
15-09:37	S	K'	1.948 - 2.299	25 x 120	178.9	0.167		
16-10:40	I	K'	1.948 - 2.299	3 x 30	202.6	0.294	6.33e-5	0.0265
16-10:48	I	$H_2(\nu = 1 - 0)$	2.111 - 2.145	4 x 60	202.7	0.295	9.90E-4	0.0240
16-10:55	I	Brγ	2.152 - 2.185	3 x 60	202.8	0.296	1.07E-3	0.0114
16-11:06	I	FeII	1.633 - 1.658	3 x 60	203.0	0.296	4.83e-4	0.0149
16-11:14	I	CH_4L	1.613 - 1.749	4 x 30	203.2	0.297	8.64e-5	0.0144
16-11:52	I	H	1.485 - 1.781	19 x 5	203.7	0.300	3.66e-5	0.0324
16-11:52	S	H	1.485 - 1.781	19 x 120	203.7	0.300		
17-10:40	I	K'	1.948 - 2.299	4 x 30	225.3	0.415	6.40e-5	0.0261
17-10:46	I	$H_2(\nu = 1 - 0)$	2.111 - 2.145	3 x 60	225.4	0.416	1.00e-3	0.02326
17-10:52	I	Brγ	2.152 - 2.185	3 x 60	225.5	0.416	1.08e-3	0.0113
17-10:58	I	FeII	1.633 - 1.658	3 x 60	225.6	0.417	4.73e-4	0.0138
17-11:03	I	CH_4L	1.613 - 1.749	3 x 30	225.7	0.417	8.60e-5	0.0132
17-11:08	I	H	1.485 - 1.781	3 x 30	225.8	0.418	3.60e-5	0.0292
17-11:54	I	K'	1.948 - 2.299	19 x 5	226.5	0.422	6.40e-5	
17-11:54	S	K'	1.948 - 2.299	19 x 120	226.5	0.422		
17-13:32	I	H	1.485 - 1.781	4 x 5	228.0	0.430	3.60e-5	
17-13:32	S	H	1.485 - 1.781	4 x 120	228.0	0.430		

1 : Approximate starting time (UT).
2 : I for images; S for spectra.
3 : Number of images times the integration time in seconds
4 : Central Meridian Longitude (or sub-Earth longitude).
5 : Angle Sun-Titan-Earth; Sun is to the West of Titan on the sky.
6 : Factor with which to multiply a 1 second exposure image to convert to I/F.

For all observations, the geocentric distance $\Delta \approx 8.068 - 8.086$ AU; heliocentric distance $r_0 \approx 9.053 - 9.064$ AU; Angular diameter is 0.88"; Position angle of North Pole $PA = 353.33°$ (all images are rotated so Titan north is up).

Table 2. Additional Data Used in Figure 14

UT Date	Filters	CML (deg)	Phase angle[1]	Reference[3]
1999-Oct-30	H1702[2]	109	0.89 E	Roe et al. 2002a
2000-Aug-17	H1702	208	6.34 E	Roe et al. 2002a
2001-Jan-11	H1702	285	5.19 W	this paper
2001-Feb-19	H1702	106	6.20 W	this paper
2001-Feb-20	H1702	108	6.19 W	Roe et al. 2002a
2001-Dec-18	$H_2(\nu = 1-0)$, Brγ	47	1.74 W	Roe et al. 2002b
2001-Dec-20	$H_2(\nu = 1-0)$, Brγ	93	1.97 W	Roe et al. 2002b
2003-Jan-26	$H_2(\nu = 1-0)$	154	4.28 W	this paper
2003-Mar-09	$H_2(\nu = 1-0)$	21	6.29 W	this paper
2003-Oct-11	$H_2(\nu = 1-0)$	204	6.33 E	Team Keck
2003-Oct-12	$H_2(\nu = 1-0)$	227	6.32 E	Team Keck
2003-Nov-11	Brγ	186	5.57 E	Schaller *et al.* 2005
2003-Nov-12	Brγ	208	5.44 E	Schaller *et al.* 2005
2003-Nov-13	Brγ	231	5.37 E	Schaller *et al.* 2005
2003-Nov-14	Brγ	254	5.28 E	Schaller *et al.* 2005
2003-Nov-18	$H_2(\nu = 1-0)$, Brγ	344	4.60 E	Team Keck
2003-Nov-29	Brγ	230	3.91 E	Schaller *et al.* 2005
2003-Dec-10	$H_2(\nu = 1-0)$, Brγ	121	2.50 E	Team Keck
2003-Dec-15	$H_2(\nu = 1-0)$, Brγ	232	1.94 E	Team Keck
2003-Dec-17	$H_2(\nu = 1-0)$, Brγ	277	1.71 E	Team Keck
2003-Dec-18	$H_2(\nu = 1-0)$, Brγ	300	1.60 E	Team Keck
2003-Dec-24	Brγ	74	0.95 E	Schaller *et al.* 2005
2003-Dec-25	Brγ	97	0.83 E	Schaller *et al.* 2005
2003-Dec-26	Brγ	120	0.70 E	Schaller *et al.* 2005
2003-Dec-27	Brγ	142	0.56 E	Schaller *et al.* 2005
2004-Jan-10	$H_2(\nu = 1-0)$, Brγ	98	1.13 W	Schaller *et al.* 2005
2004-Sep-02	$H_2(\nu = 1-0)$, Brγ	17	4.65 E	Team Keck
2004-Sep-28	$H_2(\nu = 1-0)$, Brγ	240	5.97 E	Team Keck
2004-Oct-02	$H_2(\nu = 1-0)$, Brγ	331	6.08 E	Team Keck
2004-Oct-03	$H_2(\nu = 1-0)$	354	6.11 E	Team Keck
2004-Oct-07	Brγ	84	6.45 E	Schaller *et al.* 2005
2004-Oct-23	$H_2(\nu = 1-0)$, Brγ	84	6.30 E	Team Keck
2004-Nov-02	$H_2(\nu = 1-0)$, Brγ	310	6.10 E	Team Keck
2004-Nov-03	$H_2(\nu = 1-0)$, Brγ	332	6.13 E	Team Keck
2004-Nov-27	$H_2(\nu = 1-0)$, Brγ	155	4.90 E	Team Keck
2005-Jan-20	$H_2(\nu = 1-0)$, Brγ	294	0.772 W	Team Keck
2005-Feb-14	$H_2(\nu = 1-0)$, Brγ	136	3.51 W	this paper
2005-Feb-15	$H_2(\nu = 1-0)$, Brγ	159	3.61 W	this paper
2005-Feb-25	$H_2(\nu = 1-0)$, Brγ	25	4.49 W	Team Keck

1 : Phase angle, and direction of the Sun on the sky (West, East), relative to Titan.
2 : Wavelength range: 1.67 - 1.73 μm.
3 : Team Keck data are available on: http://www2.keck.hawaii.edu/science/titan/.

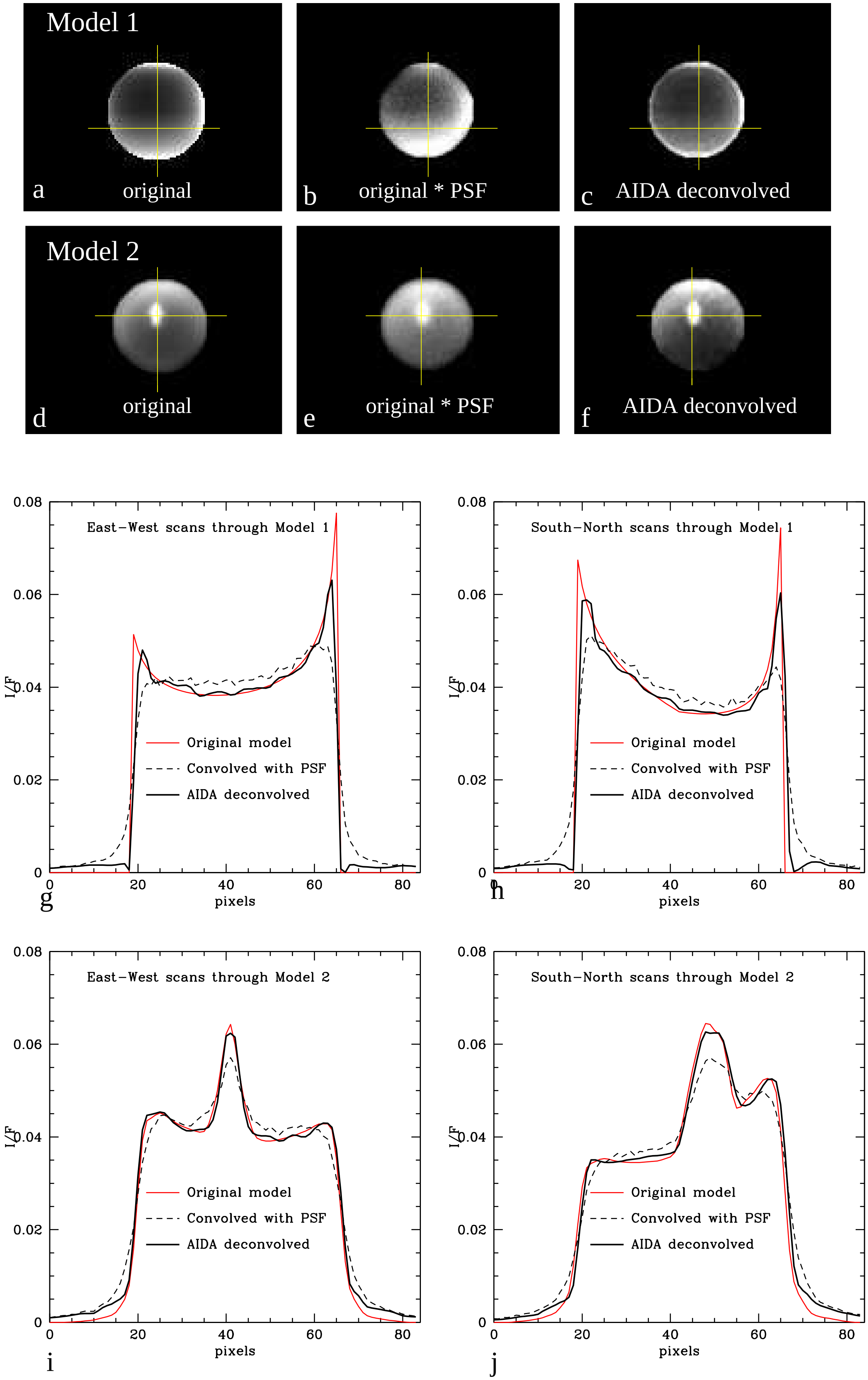
Model 1
a original
b original * PSF
c AIDA deconvolved
Model 2
d original
e original * PSF
f AIDA deconvolved
East−West scans through Model 1
South−North scans through Model 1
East−West scans through Model 2
South−North scans through Model 2
Original model
Convolved with PSF
AIDA deconvolved
I/F
pixels
0
0.02
0.04
0.06
0.08
20
40
60
80
g
h
i
j

Fig. 1

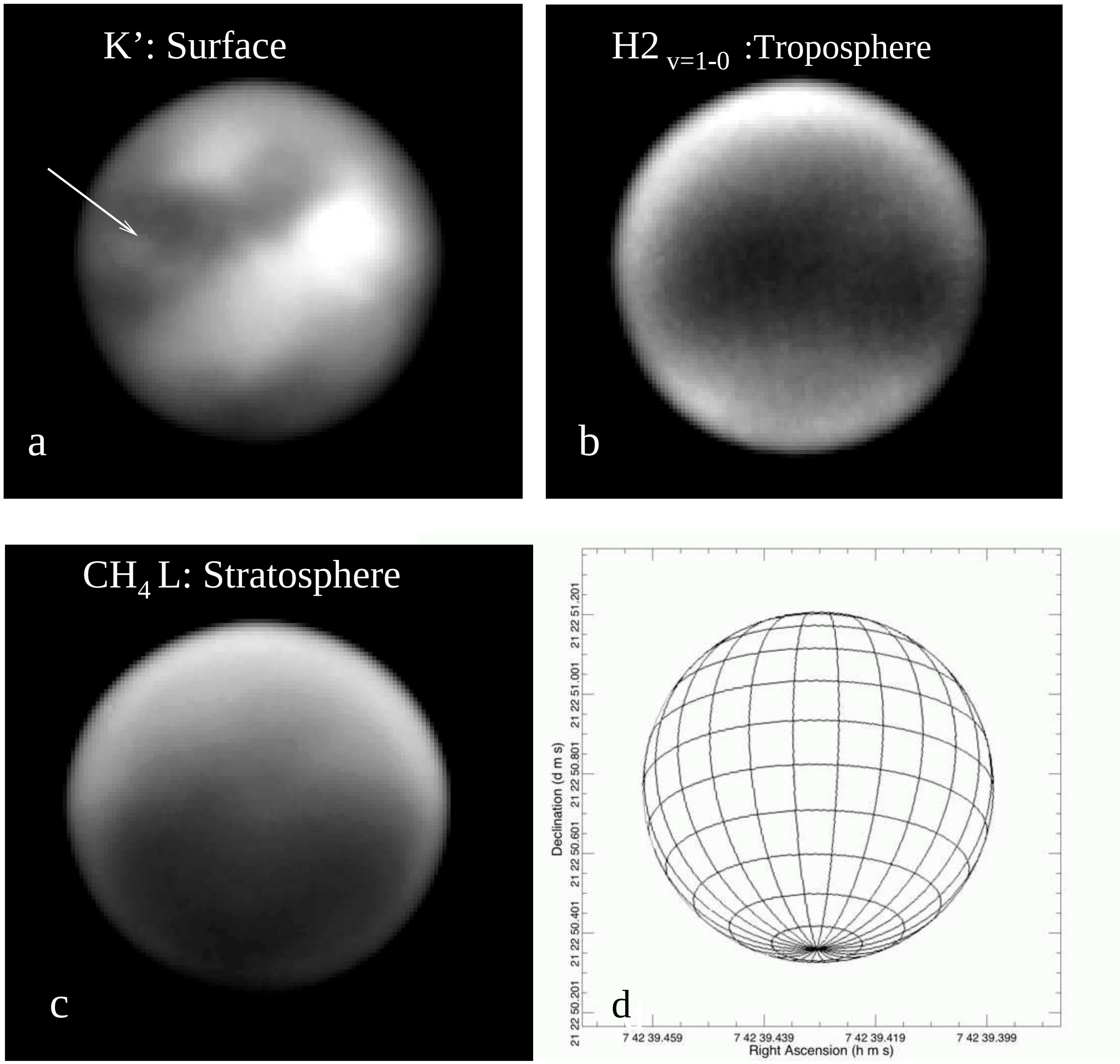
K': Surface
a
H2 v=1-0 :Troposphere
b
CH4 L: Stratosphere
c
d
Declination (d m s)
21 22 50.201
21 22 50.401
21 22 50.601
21 22 50.801
21 22 51.001
21 22 51.201
7 42 39.459
7 42 39.439
7 42 39.419
7 42 39.399
Right Ascension (h m s)

Fig. 2

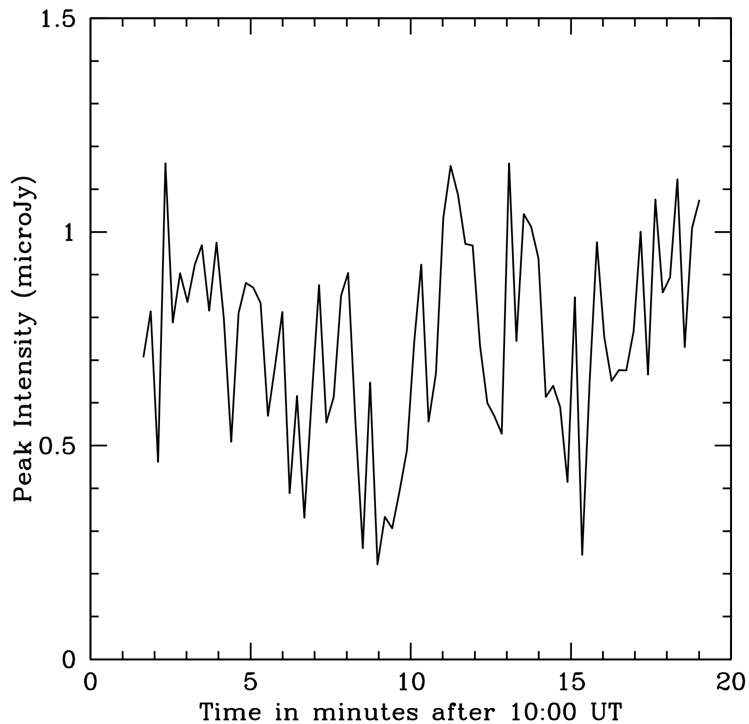
1.5
1
0.5
0
0
5
10
15
20
Peak Intensity (microJy)
Time in minutes after 10:00 UT

Fig. 3

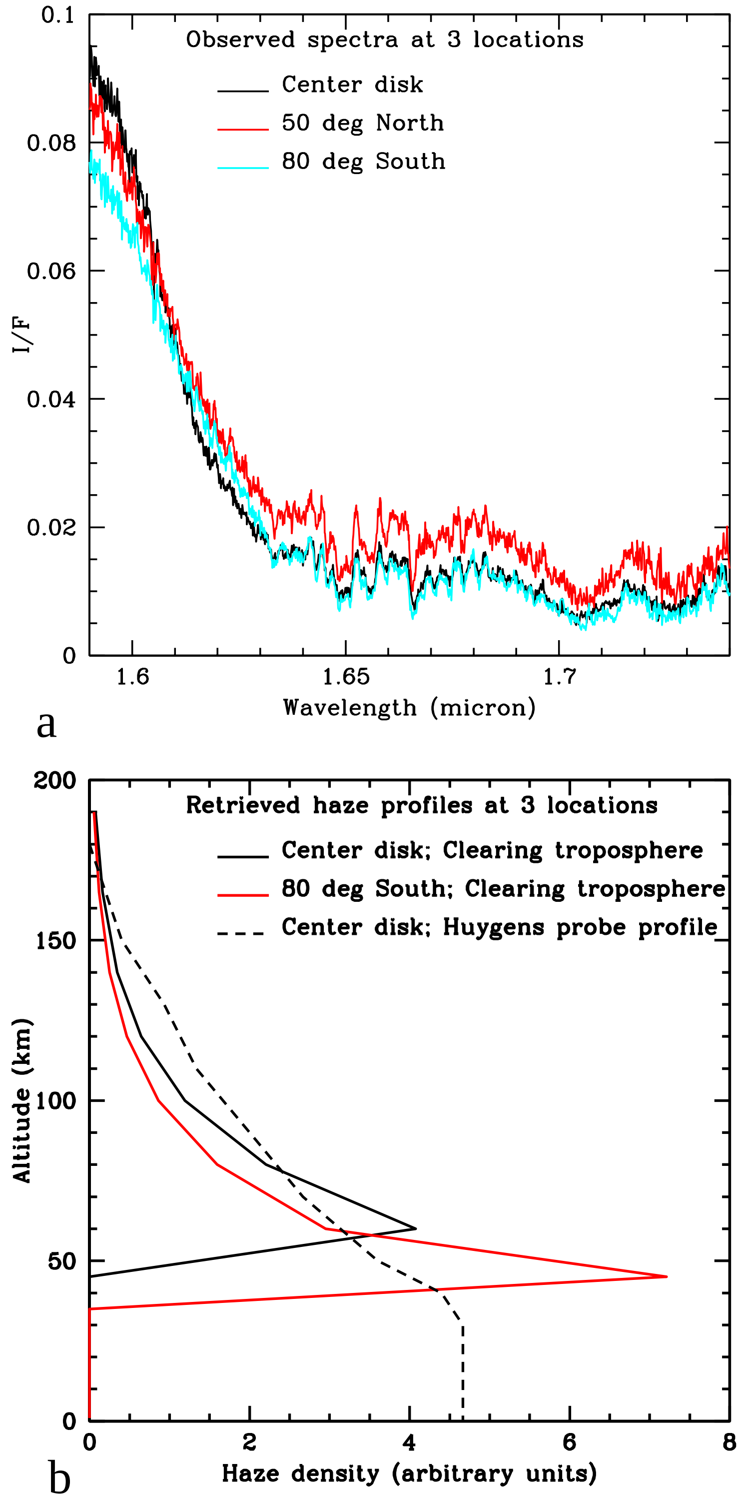

Observed spectra at 3 locations
Center disk
50 deg North
80 deg South
I/F
Wavelength (micron)
0.1
0.08
0.06
0.04
0.02
0
1.6
1.65
1.7
a
Retrieved haze profiles at 3 locations
Center disk; Clearing troposphere
80 deg South; Clearing troposphere
Center disk; Huygens probe profile
Altitude (km)
Haze density (arbitrary units)
200
150
100
50
0
2
4
6
8
b

Fig. 4

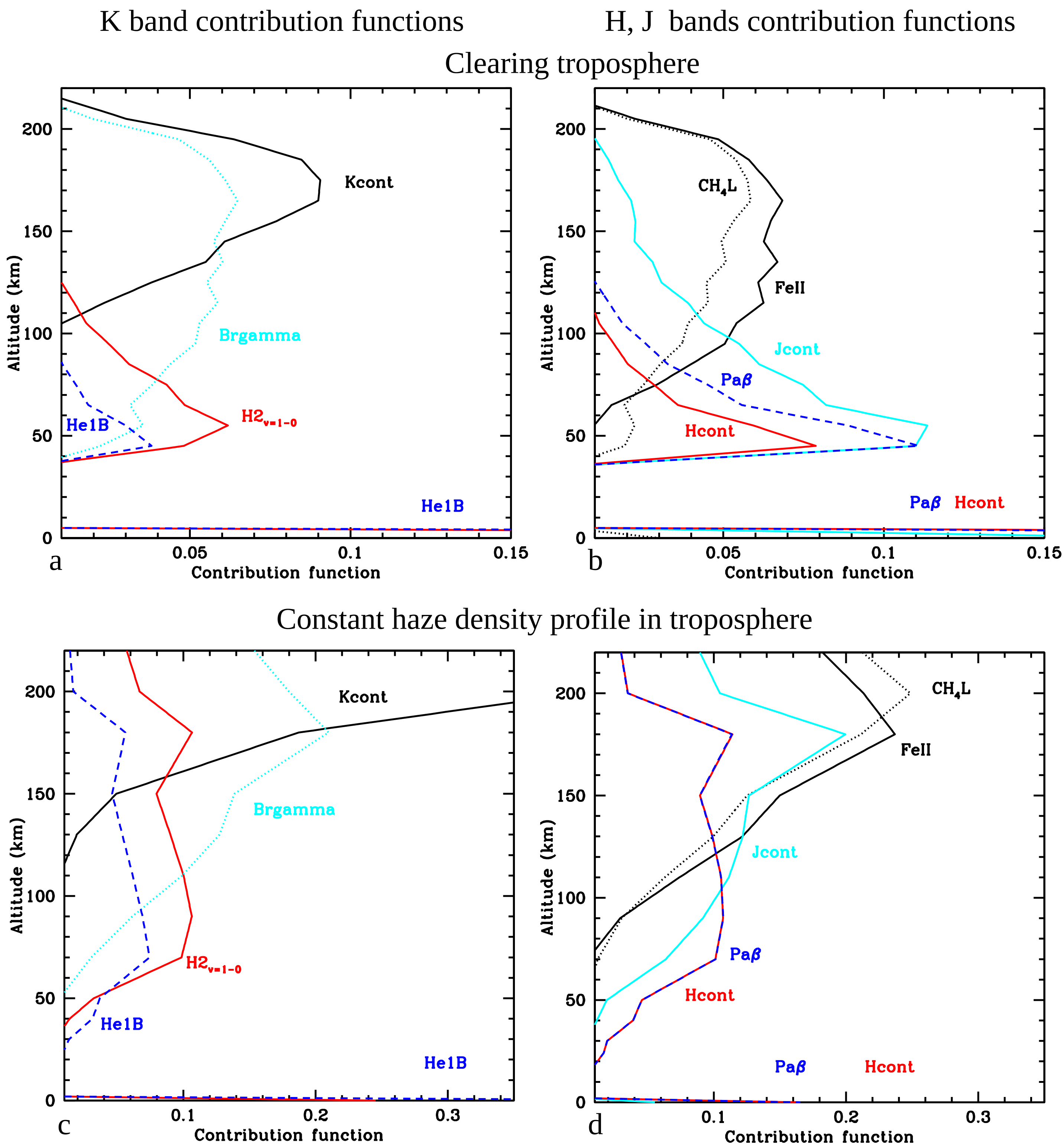
K band contribution functions
H, J bands contribution functions
Clearing troposphere
Kcont
Brgamma
H2v=1-0
He1B
He1B
Altitude (km)
Contribution function
a
CH4L
FeII
Jcont
Paβ
Hcont
Paβ Hcont
Altitude (km)
Contribution function
b
Constant haze density profile in troposphere
Kcont
Brgamma
H2v=1-0
He1B
He1B
Altitude (km)
Contribution function
c
CH4L
FeII
Jcont
Paβ
Hcont
Paβ Hcont
Altitude (km)
Contribution function
d

Fig. 5

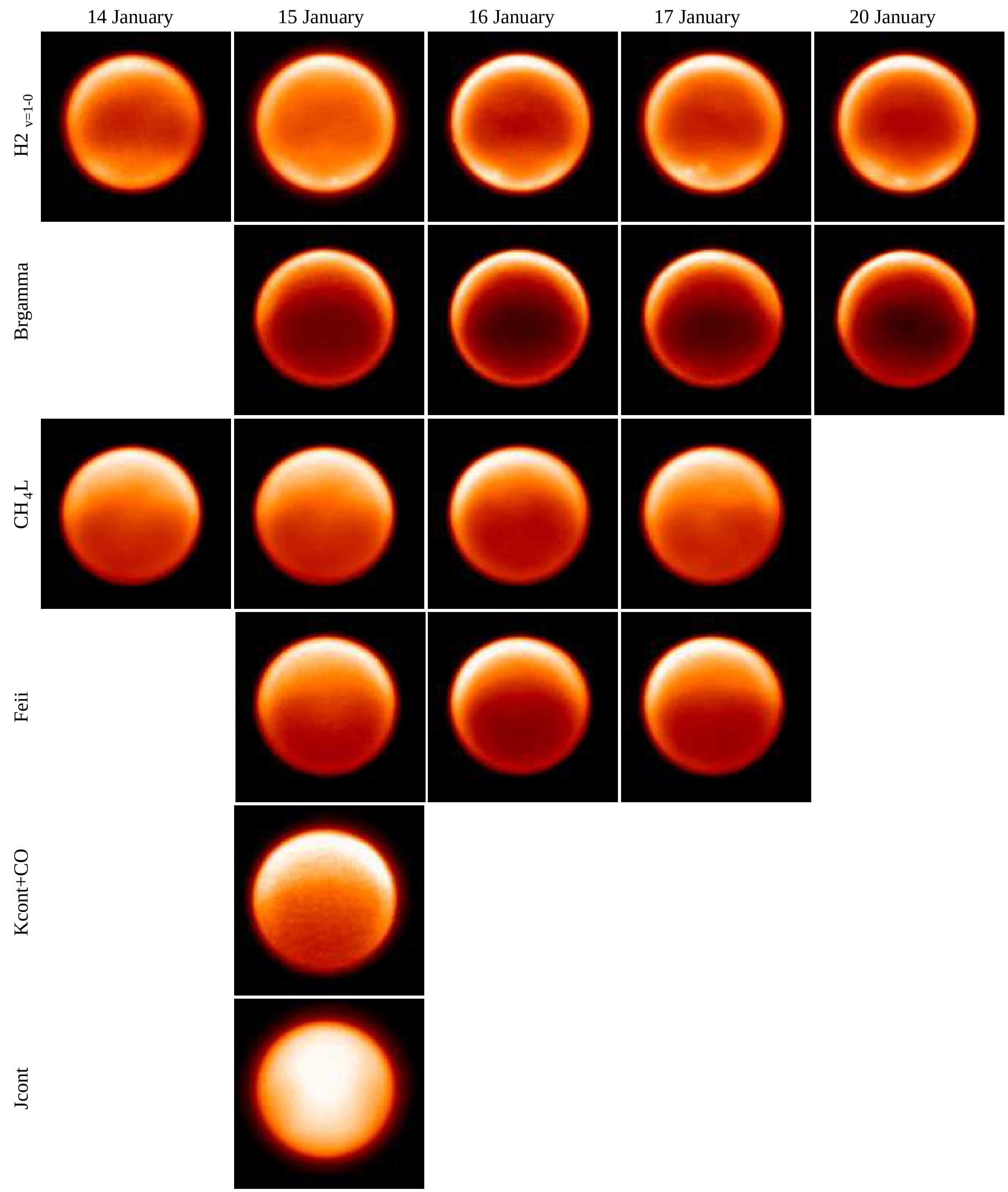

14 January
15 January
16 January
17 January
20 January
H2 v=1-0
Brgamma
CH4L
Feii
Kcont+CO
Jcont

Fig. 6

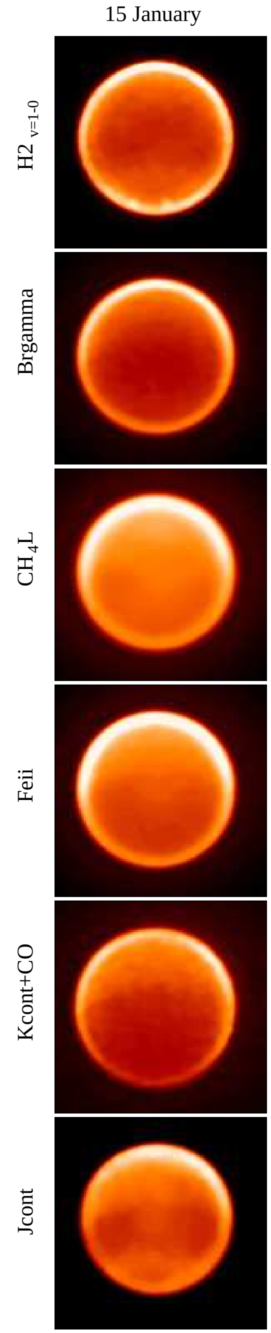

Fig. 7

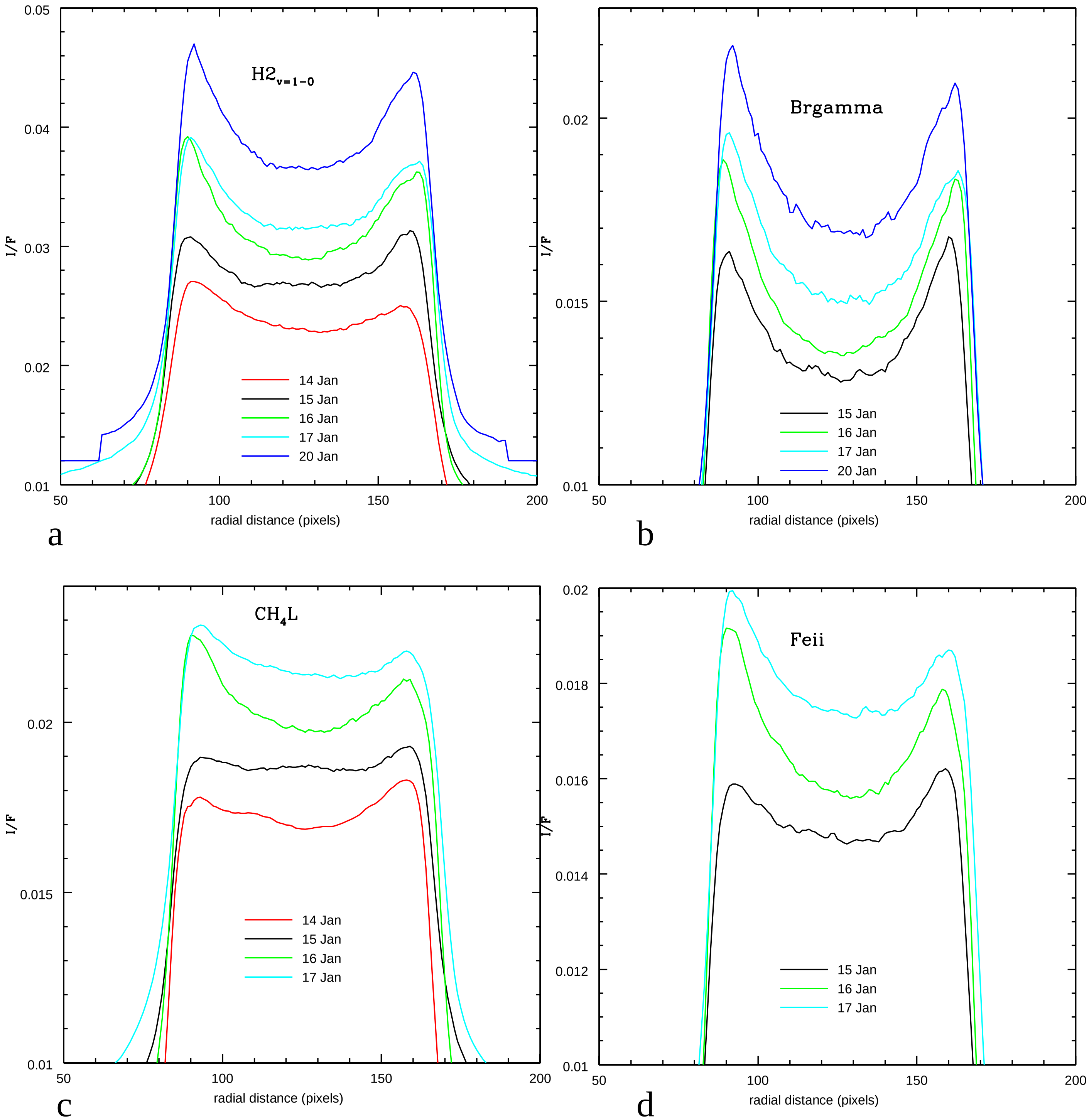
H2v=1-0
14 Jan
15 Jan
16 Jan
17 Jan
20 Jan
I/F
radial distance (pixels)
a
Brgamma
15 Jan
16 Jan
17 Jan
20 Jan
b
CH4L
c
Feii
d

Fig. 8

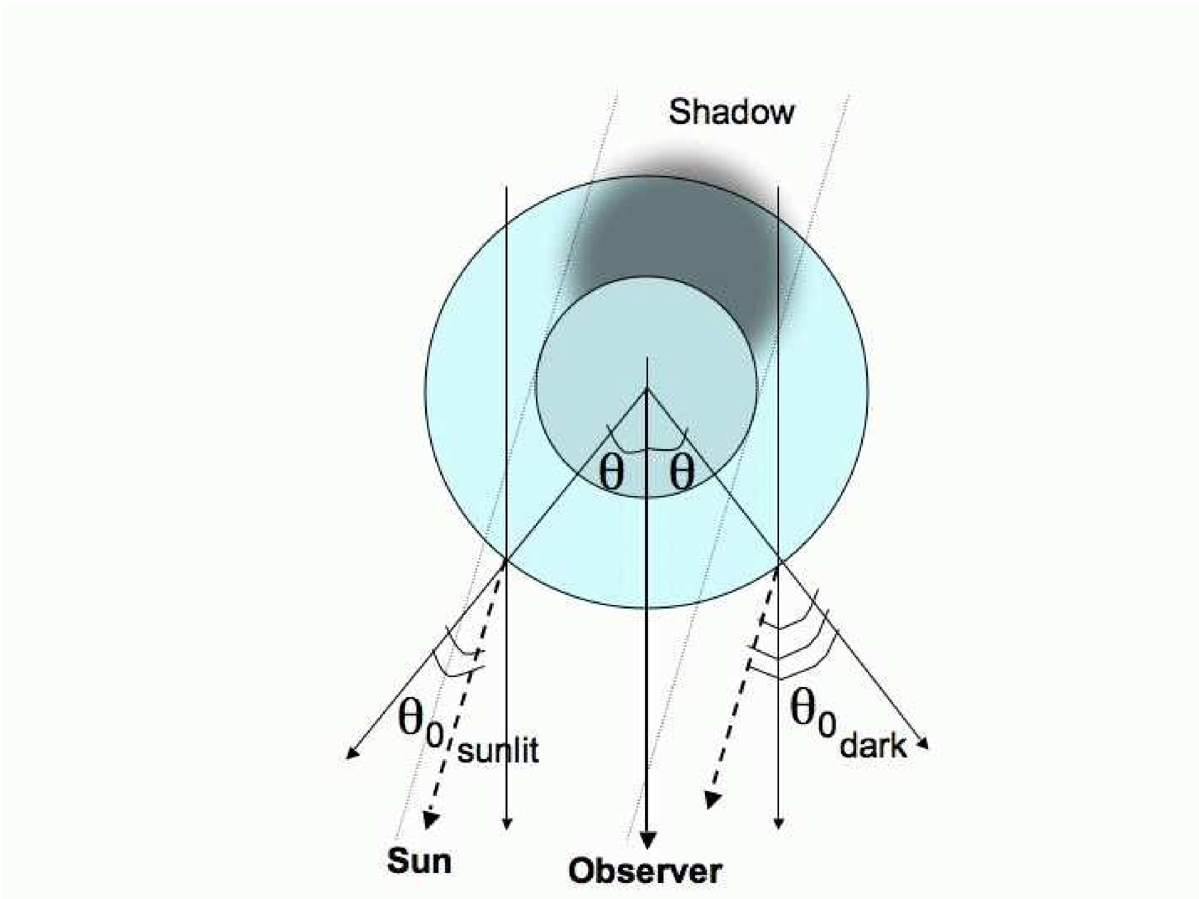

Fig. 9

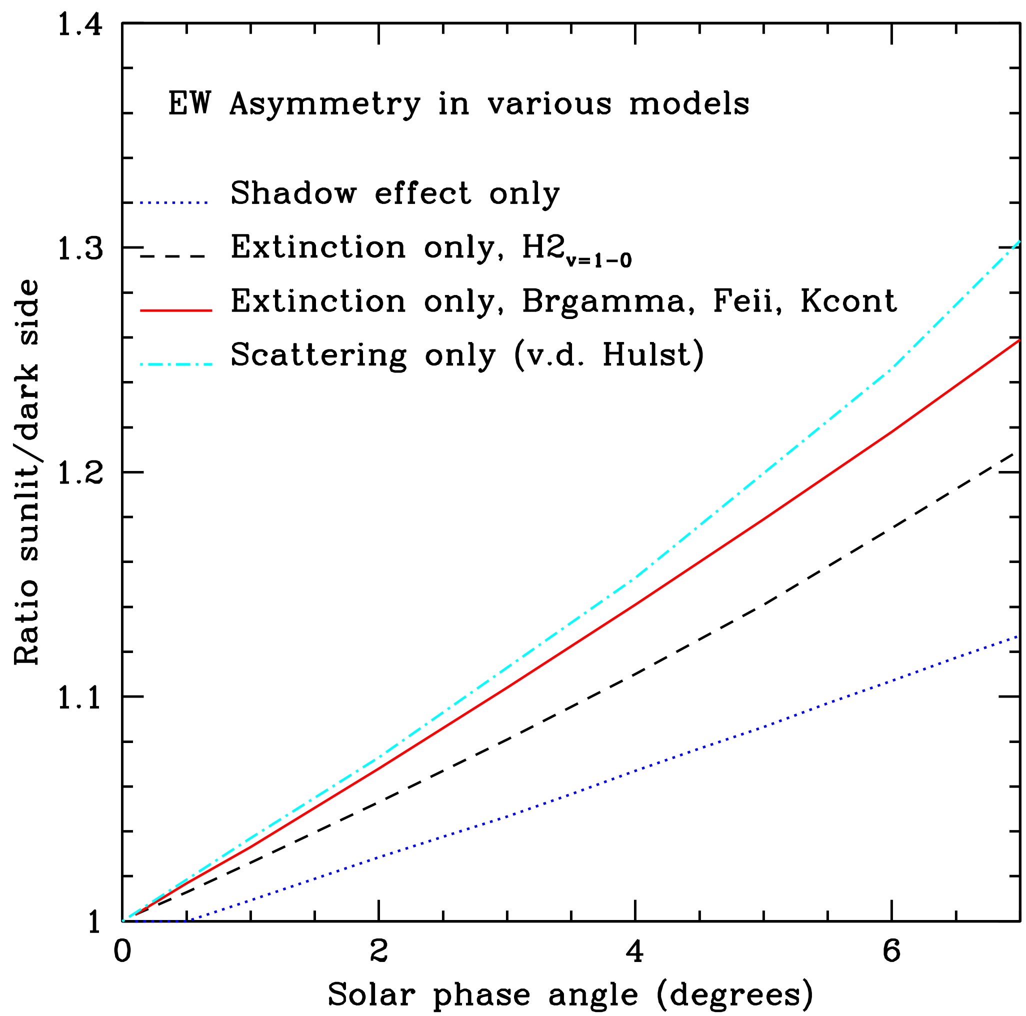
EW Asymmetry in various models
Shadow effect only
Extinction only, H2v=1-0
Extinction only, Brgamma, Feii, Kcont
Scattering only (v.d. Hulst)
Ratio sunlit/dark side
Solar phase angle (degrees)
1.4
1.3
1.2
1.1
1
0
2
4
6

Fig. 10

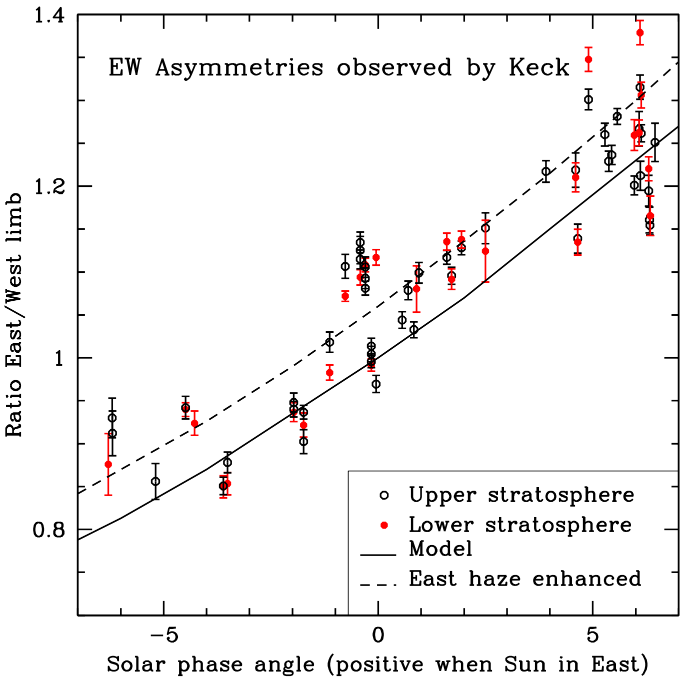
EW Asymmetries observed by Keck
Ratio East/West limb
Solar phase angle (positive when Sun in East)
Upper stratosphere
Lower stratosphere
Model
East haze enhanced
1.4
1.2
1
0.8
−5
0
5

a

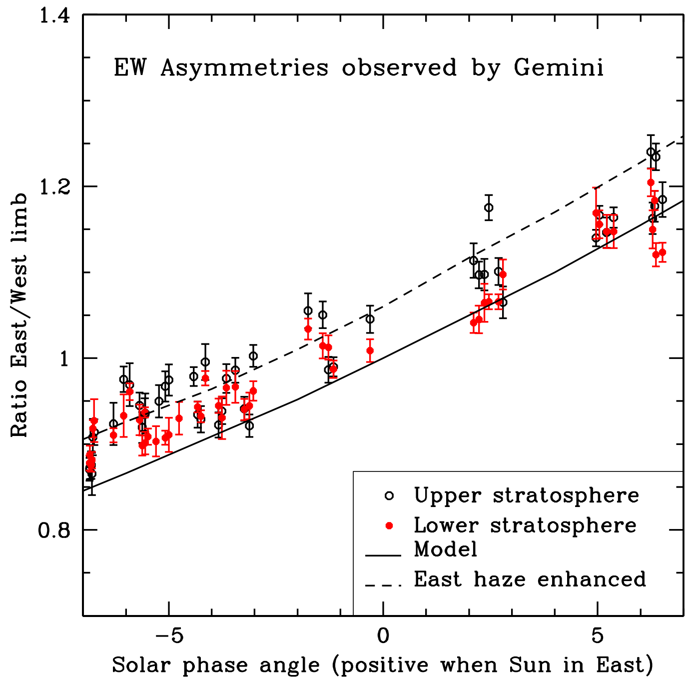
EW Asymmetries observed by Gemini
Ratio East/West limb
Solar phase angle (positive when Sun in East)
Upper stratosphere
Lower stratosphere
Model
East haze enhanced
1.4
1.2
1
0.8
−5
0
5

b

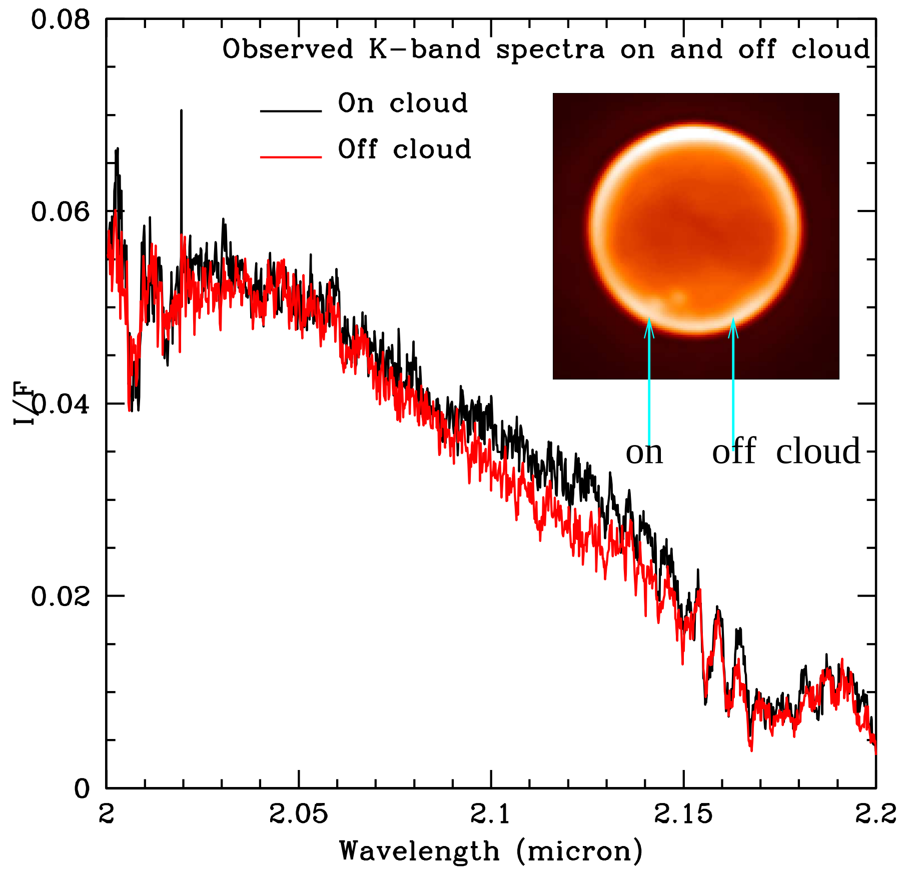

Observed K-band spectra on and off cloud
On cloud
Off cloud
on
off cloud
I/F
0.08
0.06
0.04
0.02
0
2
2.05
2.1
2.15
2.2
Wavelength (micron)

Fig. 12

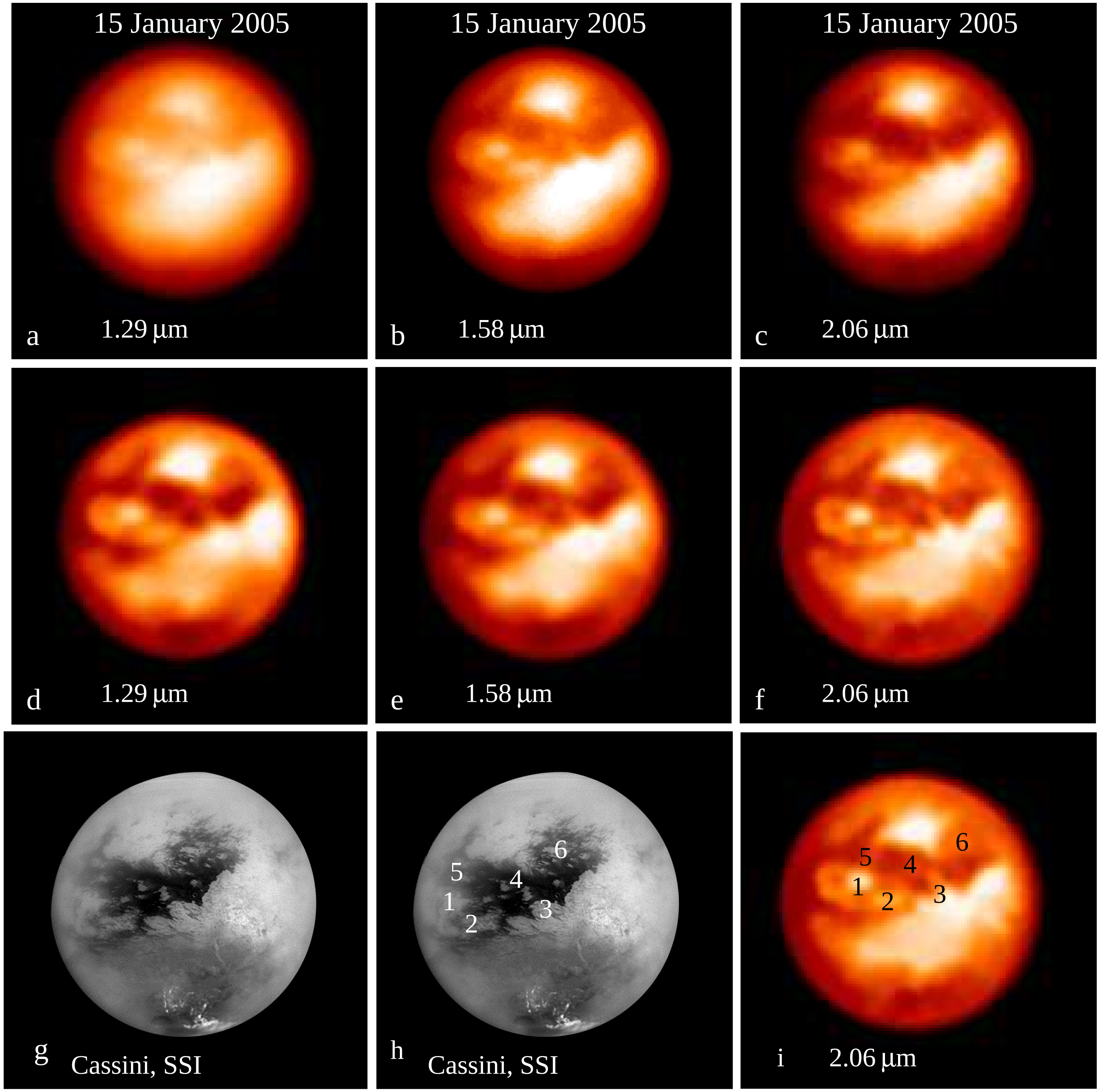
15 January 2005
15 January 2005
15 January 2005
a
1.29 µm
b
1.58 µm
c
2.06 µm
d
1.29 µm
e
1.58 µm
f
2.06 µm
g
Cassini, SSI
h
Cassini, SSI
5
1
2
4
3
6
i
2.06 µm
5
4
6
1
2
3

Fig. 13

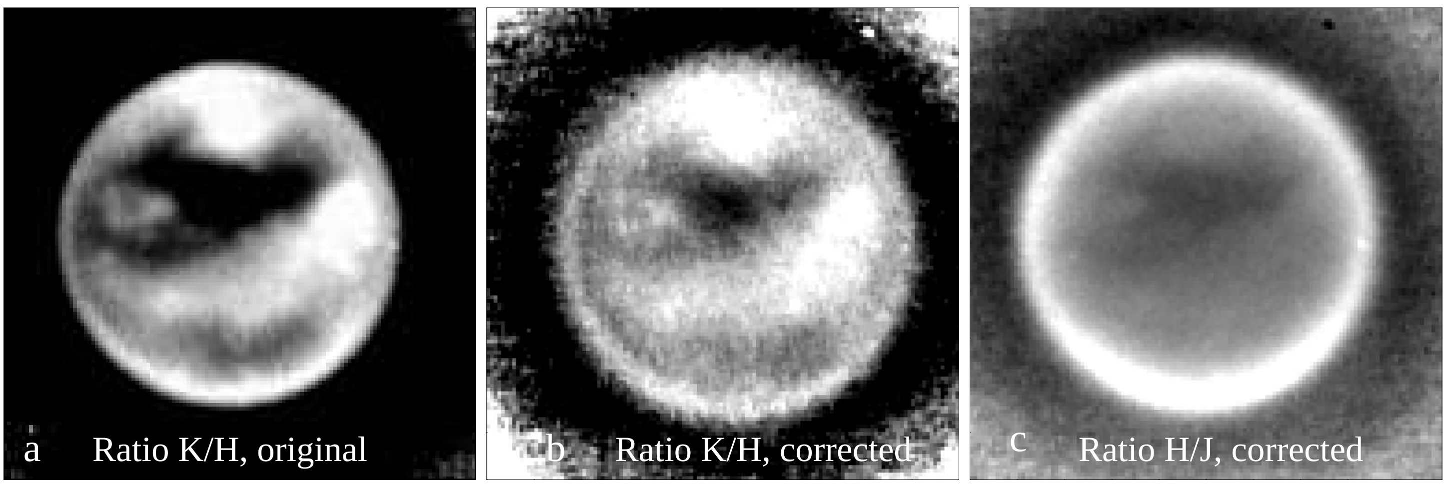
a
Ratio K/H, original
b
Ratio K/H, corrected
c
Ratio H/J, corrected

Fig. 14